Stratigraphic expression of the human impacts in condensed deposits of the Northern Adriatic Sea

Michaela Berensmeier[1]*, **Adam Tomašových[2]**, **Rafał Nawrot[1]**,
Daniele Cassin[3], **Roberto Zonta[3]**, **Ivana Koubová[2]** and **Martin Zuschin[1]**

[1]University of Vienna, Josef-Holaubek-Platz 2, 1090 Vienna, Austria

[2]Earth Science Institute, Slovak Academy of Sciences, Dúbravska cesta 9, 84005 Bratislava, Slovakia

[3]Consiglio Nazionale delle Ricerche, Istituto di Scienze Marine, Castello 2737/F, 30122 Venice, Italy

MB, 0000-0002-8942-2917; AT, 0000-0002-0471-9480; RN, 0000-0002-5774-7311; DC, 0000-0001-7517-7597; RZ, 0000-0003-3308-9470; IK, 0000-0002-7765-7823; MZ, 0000-0002-5235-0198

*Correspondence: michaela.berensmeier@univie.ac.at

Abstract: Evaluating the history of human impacts on marine ecosystems based on sediment cores is challenging on shelves characterized by very slow sedimentation. To assess the stratigraphic expression of such impacts in the condensed deposits of an epicontinental sea, we analysed a 3 m-long core collected at 31 m water depth off the Po prodelta in the Northern Adriatic Sea by integrating geochronological (^{14}C and ^{210}Pb), sedimentological, geochemical and palaeontological proxies. A depositional history of the last 10 000 years is expressed in four different facies: (1) alluvial floodplain, (2) transitional, shell-poor silts, (3) a condensed 30 cm-thick shell lag, and (4) a 10 cm-thick layer of distal prodelta silts comprising the last *c.* 500 years. 10 000-year-old shells of *Lentidium mediterraneum* spread over the shell lag and prodelta sediments document onshore transport during the early Holocene sea-level rise. *Varicorbula gibba* shells are age-homogeneous within the subsurface shell lag, documenting decimetre-scale mixing by bioturbation in the past. However, in spite of low sedimentation rates, the organic and heavy metal enrichment, the increase in proportional abundance of benthic foraminifers preferring organic-rich sediments (*Nonionella* sp.), and the increase in size of molluscs (*V. gibba*) in the upper 10 cm formed by prodelta silts still detect the eutrophication in this region during the twentieth century. These eutrophication proxies are preserved in the stratigraphic record owing to temporarily increasing sedimentation rate and decreasing mixing depth.

Supplementary material: Bulk geochemistry data including *p*-values, Pearson correlation values and PCA loadings are provided as supplementary material (S1). Furthermore, results of age dating (S2), micro-X-ray fluorescence core scanning (S3), palaeobiological data (species list) (S4) and shell size data of *Varicorbula gibba* (S5) are provided as supplementary materials. All files are available at https://doi.org/10.6084/m9.figshare.c.6342805

Holocene marine sediments archive sea-level, oceanographic and ecosystem changes that occurred since the Last Glacial Maximum in the Late Pleistocene. Therefore, they have the potential to incorporate signals of human impacts that occurred over the past centuries and decades (Rabalais *et al.* 2007; Dolven *et al.* 2013). The deposition of sediments on continental shelves depends on the tectonic setting, climate, and the distance to active sedimentary sources, and can be subjected to sediment starvation and winnowing, especially during sea-level rise (e.g. Schlager 1993; Cattaneo and Steel 2003; Föllmi 2016). Low net sedimentation rates lead to stratigraphic condensation and high time-averaging of sedimentary particles and fossils, compromising the temporal resolution of the stratigraphic record (Kowalewski 1996; Kidwell 2013). These condensation effects can complicate reconstructions of baseline conditions prior to human impacts and inhibit inferences about the timing and rate of ecosystem shifts over the past decades or centuries (Kosnik *et al.* 2007; Tomašových *et al.* 2020; Nawrot *et al.* 2022). Difficulties thus arise while disentangling the human impact from natural changes based on the stratigraphic record (e.g. Wolfe *et al.* 2013; Fairchild *et al.* 2019). Regardless of debates about the formal definition of the Anthropocene (Lewis and Maslin 2015; Gibbard *et al.* 2022), here it refers to an informal time interval during which human activities significantly impacted biogeochemical cycles, depositional processes, and ecosystem functioning and ultimately left distinct signatures of these impacts in the stratigraphic record.

Depositional conditions characterized by low net sedimentation rates can result from (1) alternation of omission episodes with episodes of relatively faster sedimentation (leading to stratigraphic increments with limited time-averaging separated by hiatuses), or (2) very slow but relatively persistent sedimentation that can be coupled with intense mixing by bioturbation. The first scenario may alter the record of gradual environmental changes into abrupt stratigraphic changes in geochemical and biotic proxies (via hiatuses); whereas the second scenario induces smearing of initially rapid environmental changes into more gradual stratigraphic shifts. These scenarios can be distinguished with radiocarbon- or U–Th-based dating that quantify frequency distributions of ages of skeletal particles, allowing explicit estimation of time-averaging and stratigraphic resolution of the Holocene stratigraphic record (Flessa *et al.* 1993; Kosnik *et al.* 2007; Scarponi *et al.* 2013; Tomašových *et al.* 2014, 2021). Therefore, the use of chemostratigraphic or biotic proxies for palaeoenvironmental reconstructions can be assessed through analyses of sediments that integrate geochronological, geochemical and palaeoecological methods

(Kowalewski 1996; Patzkowsky and Holland 2012; Kidwell 2013; Wilkinson *et al.* 2014; Kuzyk *et al.* 2015).

In this study, we investigate the Holocene strata comprising the last *c.* 10 000 years deposited in the central part of the Northern Adriatic Sea, the northernmost sub-basin of the Mediterranean Sea (Fig. 1). In contrast to high sedimentation sites within the mud-belt of the Po Delta (Barmawidjaja *et al.* 1995; Scarponi *et al.* 2013; Tomašových *et al.* 2018), the sampling site is located in the distal part of the Po prodelta (on the transition to the wave-dominated shelf segment of the Northern Adriatic Sea) that tends to be exposed to significant stratigraphic condensation (Correggiari *et al.* 1996*a*; Picone *et al.* 2008). The location investigated here is formed by silty sediments deposited in low-energy environments well below fair-weather wave base, situated *c.* 30 km in distance to the Po River mouth (Fig. 1). This site can differ in its potential to archive signals of human impacts relative to other condensed sites with coarser sediments and stronger exposure to currents in the eastern parts of the Northern Adriatic Sea (Gallmetzer *et al.* 2019; Tomašových
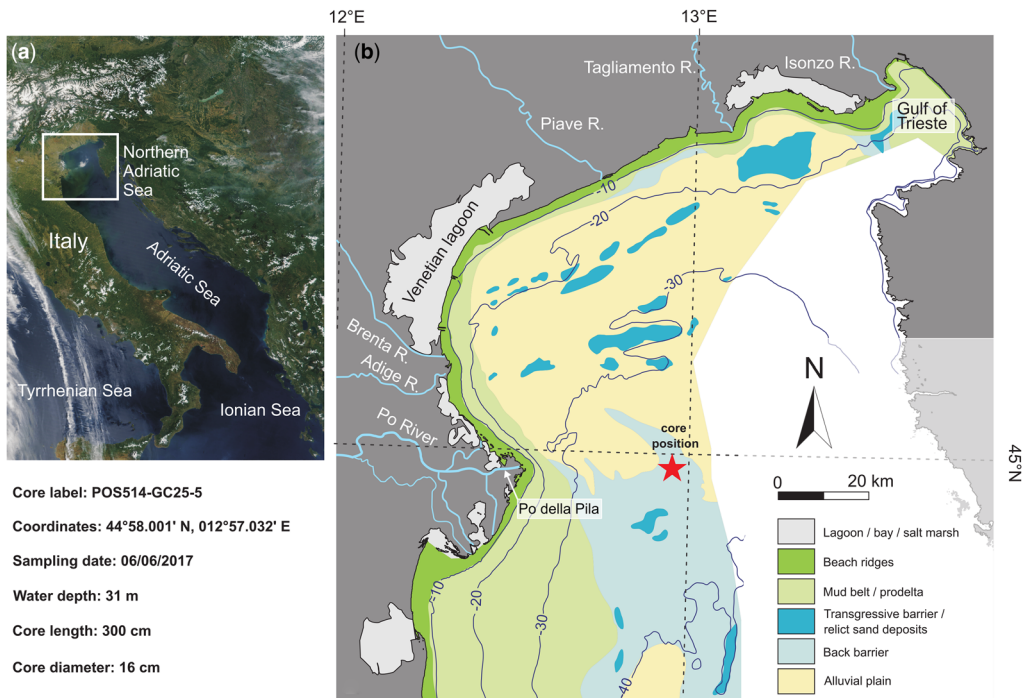
Fig. 1. Sampling station in the Northern Adriatic Sea. (**a**) Satellite image of Italy and its surrounding sub-basins of the Mediterranean Sea. MODIS satellite image (Terra) of the northern Adriatic coast, collected on day 335, 2002, at 1030 Greenwich Mean Time (GMT). (**b**) Geological map based on maps of the Geological Survey of Italy. Note that offshore muds cover alluvial and brackish deposits in some parts of the basin, but are not displayed here. Source: (a) https://eoimages.gsfc.nasa.gov/images/imagerecords/59000/59211/Italy.A2002138.1010.250m.jpg; (b) map of Venice, Trincardi *et al.* (2002) and map of Ravenna, Trincardi and Argagni (2003).

et al. 2019; Nawrot *et al.* 2022). Here, we quantify the stratigraphic resolution, we measure time-averaging recorded by skeletal particles, and we trace stratigraphic signals of human activities based on geochemical proxies and abundance of molluscs, foraminifers and ostracods.

The Northern Adriatic Sea provides a good opportunity for assessing the stratigraphic expression of marine ecosystems altered by human impacts because: (1) the basin evolution during the Holocene is well documented (Amorosi *et al.* 2008; Trincardi *et al.* 2011; Campo *et al.* 2017); and (2) the stratigraphic record of human impact during the nineteenth and twentieth centuries (with the main impacts represented by trawling, overfishing, eutrophication, and pollution) is well preserved and independently documented in cores at sites with high sedimentation rates at the Po Delta or in the northern Gulf of Trieste. These core-based studies documented a major mid-twentieth century shift from baseline macrobenthic communities with molluscs and echinoderms sensitive to seasonal oxygen depletion and sediment disturbances towards the states impacted by hypoxic events, trawling and other disturbances that intensified during the late twentieth century (Barmawidjaja *et al.* 1995; Rossi and Vaiani 2008; Vidovic *et al.* 2016; Albano *et al.* 2018; Tomašových *et al.* 2018, 2020; Gallmetzer *et al.* 2019; Salvi *et al.* 2020; Haselmair *et al.* 2021).

The Northern Adriatic Sea during the Holocene

The Northern Adriatic Sea is characterized by a low-gradient shelf separating the Italian and the Balkan Peninsulas (Fig. 1). This Mediterranean sub-basin exhibits geographically variable nutrient supply, primary productivity, and sedimentation rates (Frignani *et al.* 2005; Zuschin and Stachowitsch 2009). On one hand, sedimentation rate is high close to river-borne sediment supply in the western parts ($c.$ 1–2 cm a^{-1}, Frignani and Langone 1991; Palinkas and Nittrouer 2007; Alvisi 2009; Tomašových *et al.* 2018). On the other hand, much lower net sedimentation rates characterize the sediment-starved settings in the central part of the Gulf of Trieste ($<$0.3 cm a^{-1} in Ogorelec *et al.* 1991; Novak *et al.* 2020; and even $<$0.01 cm a^{-1} in Tomašových *et al.* 2019, 2021). The central portions of the Northern Adriatic Sea, including our sampling site, are affected by sediment winnowing induced by high-energy currents, which are driven by an overall counter-clockwise cyclonic circulation with a wave-dominated microtidal regime (Trincardi *et al.* 1994). In these areas, relict sediments deposited during the transgressive phase are often preserved at or just beneath the sediment–water interface (Picone *et al.* 2008; Spagnoli *et al.* 2014; Moscon 2016).

The Northern Adriatic Sea is a young, shallow shelf sea with the maximum water depth of 50 m that was formed during the Holocene transgression (Amorosi *et al.* 2017). In the early Holocene, the sea level rose rapidly and in steps during the major deglaciation phase *c.* 12 000 and 7500 years BP (before present, e.g. Lambeck *et al.* 2014). Between 10 500 and 9000 years BP, fluvial and coastal environments rimmed the northern part of the Adriatic Basin (Amorosi *et al.* 2003, 2008). The subsequent marine flooding of the flat northern Adriatic shelf led to the formation of barrier-lagoon systems (Fabbri *et al.* 2001; Storms *et al.* 2008). The maximum flooding and maximum shoreline ingression occurred in the Northern Adriatic Sea around 7000 to 5500 years BP (Trincardi *et al.* 2011; Amorosi *et al.* 2017). This phase led to the establishment of biostromes with epifaunal bivalves along the NE margin between the Brijuni Islands and the Gulf of Trieste (Gallmetzer *et al.* 2019). During the high-stand phase ($<c.$ 5500 years BP), a progradational mud wedge sourced by the Po River developed along the western coast of the Northern Adriatic Sea (Colantoni *et al.* 1979; Amorosi *et al.* 2008; Rossi and Vaiani 2008). This wedge is deflected southwards by a counter-clockwise surface current of the whole sub-basin (Boldrin *et al.* 2009). Currents in the central parts of the Northern Adriatic Sea thus induce sediment transport and bypassing leading to very low sedimentation rates and formation of thin and transient sediment veneers or even to erosion of older sediments deposited during the transgressive phase.

The magnitude and geographical extent of human impacts affecting marine environments in the Northern Adriatic Sea, documented by monitoring surveys and stratigraphic archives (sediment cores) peaked during the late twentieth century, due to increasing eutrophication, seasonal deoxygenation, trawling, overfishing and shellfish exploitation (Crema *et al.* 1991; Stachowitsch 1991; Nerlović *et al.* 2011; Giani *et al.* 2012; Haselmair *et al.* 2021), and heavy metal and organic pollution (Frascari *et al.* 1988; Marchetti *et al.* 1989; Fabbri *et al.* 2001; Covelli *et al.* 2006; Zonta *et al.* 2018). The Po River is the major source of nutrients in the Northern Adriatic Sea; its phosphorus loads lead to blooms of harmful algae, contributing also to a twentieth century increase in turbidity (Justić 1988). The high oxygen consumption by microbial respiration and water-column stratification led to increased frequency of mucilage events and seasonal bottom-water hypoxia or anoxia at depths below the seasonal thermocline (*c.* 10–30 m, Degobbis 1989; Faganeli *et al.* 1991; Justić 1991). Consequently, mass mortalities, differential recovery among benthic taxa, and differences in their sensitivity to other disturbances left distinct signatures in sediment cores, archived as

stratigraphic changes in the taxonomic and functional composition and in size structure of foraminiferal or molluscan assemblages (Barmawidjaja *et al.* 1995; Gallmetzer *et al.* 2017; Tomašových *et al.* 2018, 2021). A decline in the depth of bioturbation (even when abundance of shallow-burrowing infauna increased), and a loss of epifaunal suspension-feeders, grazers and browsers were observed in Holocene sediments at most sites in the Northern Adriatic Sea (Gallmetzer *et al.* 2019; Haselmair *et al.* 2021). Although an oligotrophication trend was observed in the Northern Adriatic Sea since the 1990s (Djakovac *et al.* 2012), this trend may not be persistent (Cozzi *et al.* 2020; Grilli *et al.* 2020), seasonal hypoxic events still recur in the Gulf of Trieste (Kralj *et al.* 2019), and macrobenthic communities remain dominated by the opportunistic bivalve *Varicorbula gibba* in the early twenty-first century.

Materials and methods

The 300 cm-long gravity core POS514-GC25-5 was taken during the *Poseidon* cruise in June 2017 in the western part of the Northern Adriatic Sea at 31 m water depth. Its sampling site is slightly off the Po prodelta, *c.* 32 km to the East of the Po della Pila mouth (Fig. 1). The core was cut into four pieces for better storage. Each piece was split into halves and opened.

Non-destructive imaging

X-ray computed tomography (CT) has been performed on each core half with a 1 mm down-core resolution using a Philips (Amsterdam, The Netherlands) MX8000 IDT 16 System with 120 kV voltage and ascanning dose of 314–393 mA. Data were processed with Horos v2.0.2 software (Horos Project, https://horosproject.org/). Average, minimum and maximum intensity projection algorithm (AIP, MinIP and MIP) have been used to detect low and high-density structures in a given sediment volume (Zonta *et al.* 2021).

Facies analysis and palaeobiological data

Facies interpretation is based on sediment parameters (grain size and geochemistry), the abundance and diversity of macro- and microfossil remains, and occurrence of other sedimentary features observed in the core. To facilitate comparison with previous regional-scale studies of the Holocene facies architecture in the subsurface of the Po coastal plain and Po Delta (e.g. Amorosi *et al.* 2017; Bruno *et al.* 2017; Campo *et al.* 2017), we used the facies classification and terminology of Amorosi *et al.*

(2017). Sequence-stratigraphic terminology is following the sequence model III of Catuneanu *et al.* (2009), where the transgressive systems tract (TST) formed under a significant increase in the accommodation space under rapid sea-level rise and the highstand systems tract (HST) formed during the progradation of the Po Delta (even when the offshore sites were subjected to winnowing). The assignment of stratigraphic increments to systems tracts is based on facies interpretation and geochronological data, and informed by the changes in the thickness and age of TST and HST units and by the duration of these units (separated by the maximum flooding surface) as documented in previous studies of seismic profiles and cores in the Gulf of Venice and Po Plain. The HST prograding wedge that is *c.* 10 m-thick in proximal portions of the mud-belt pinches out eastward over several kilometres to less than 1 m or few decimetres (below the seismic resolution) (Trincardi *et al.* 1994; Correggiari *et al.* 1996b; Amorosi *et al.* 2017; Bruno *et al.* 2017).

For palaeobiological analysis, the core was divided into 64 increments: the topmost 22.5 cm were sliced into 2.5 cm-thick increments (each with a volume of *c.* 500 cm^3) and the remaining core into 5 cm-thick increments (each *c.* 1000 cm^3). For the study of the benthic foraminiferal assemblage, subsamples of *c.* 30 cm^3 (*c.* 50 g) in the upper part (0–22.5 cm) and *c.* 60 cm^3 (*c.* 100 g) in the lower part (22.5–300 cm) of the core were taken from each core increment, and sieved through 63 μm and 1 mm mesh size. At least 300 specimens of benthic foraminifers were counted if faunal density was high enough and subsamples were split if faunal density was very high. A second subsample, varying in size from *c.* 60 cm^3 (*c.* 100 g) to *c.* 120 cm^3 (*c.* 200 g) in the lower and upper part of the core, respectively was taken from each increment and used for the analysis of ostracod assemblages. Only adult ostracods were counted in grain size fractions 125–250 μm and 250 μm–1 mm. All material >1 mm, including subsamples for foraminifers and ostracods, was used for the analysis of the macrofaunal (mostly molluscan) assemblage. Bivalves were counted if at least 50% of the shell was preserved and the hinge was present. For each bivalve species, the higher number of single valves (either right or left) was added to the number of double-valved specimens to get the number of individuals in each increment. Gastropods were counted if at least 50% of the shell was preserved and the aperture was present. Faunal density was calculated based on the identified number of individuals and the volume of the increment or subsample. Changes in absolute and proportional abundances of the most abundant species, representing the majority of the total fossil assemblage of molluscs (55%), benthic foraminifers (75%) and ostracods (75%), were analysed along

the core. Finally, we measured shell length of *V. gibba* to track its ecological dynamics not captured by changes in abundance alone. This species is a useful marker of eutrophication coupled with recurrent hypoxic events because its size increased during the late twentieth century at subtidal sites in the Northern Adriatic Sea (Tomašových *et al.* 2020). In contrast to size distributions from stratigraphic intervals preceding the twentieth century, in which larger individuals are rare or missing, size distributions with abundant individuals that exceed >10 mm in length are widespread in death assemblages formed since the mid-twentieth century. We measured the length of right valves in 708 specimens of this species collected in all core increments and additional 2011 specimens collected with six Van Veen grabs at the location where the core was sampled. We followed the approach of Fuksi *et al.* (2018), and used the reduced major axis regressions to predict the length from the width in specimens with incomplete preservation and to predict the length of the right valve from the length of the left valve.

Core chronology and time-averaging

Age dating was performed on the following four materials: (1) fifty valves of the bivalve *Varicorbula gibba* collected in the upper 30 cm of the core (Fig. 2a), (2) 15 valves of the bivalve *Lentidium mediterraneum* (Fig. 2b) collected across the upper 60 cm, (3) five subsamples collected from a 6 cm-sized boxwork rhodolith (*sensu* Basso 1998) from 3 to 9 cm, and (4) two terrestrial plant remains collected at 75 and 265 cm. The two bivalve species were selected according to their abundance (*V. gibba* is one of the dominant species) and differences in their bathymetric distribution and habitat preferences. Both species possess similar shell sizes, both are shallow-infaunal opportunistic filter-feeders, and both occur at high abundances in the Holocene successions of the Northern Adriatic Sea (Sawyer and Zuschin 2010; Scarponi *et al.* 2013; Weber and Zuschin 2013; Kowalewski *et al.* 2015). *L. mediterraneum* is most abundant in sandy sediments of river mouths, tidal flats and lagoons at depths <10 m (Simboura and Zenetos 2002; Bozzeda 2010; Weber and Zuschin 2013), and thus can be used to track the timing of transgression at our location. In contrast, *V. gibba* is most abundant in offshore-transition to offshore silty muds at depths >10 m (Hrs-Brenko 2006), and is currently one of the dominant molluscan species in living assemblages at the sampled site.

All ages are reported as calibrated years before AD 2017 – the year of sampling, which is abbreviated in the following as 'cal years AD2017'. These ages constrain the core geochronology, sedimentation rates, and its stratigraphic resolution.
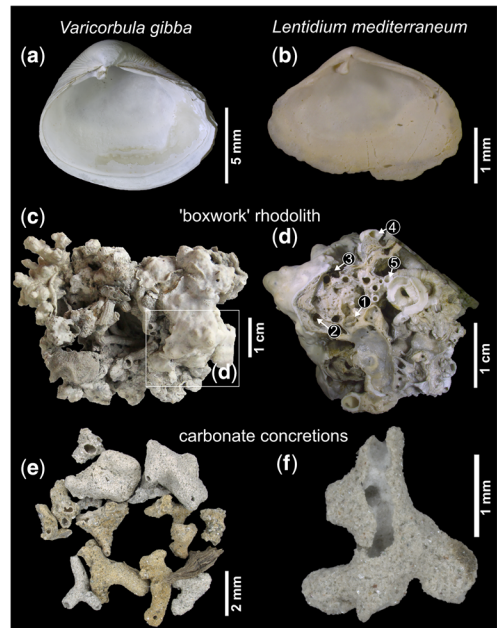
Fig. 2. Dated material and core characteristics. (**a**) *Varicorbula gibba* (170 cal years AD2017) from 0 to 2.5 cm core depth. (**b**) *Lentidium mediterraneum* from 0 to 2.5 cm core depth (9810 cal years AD2017). (**c**) Boxwork rhodolith from 3 to 9 cm core depth. (**d**) Cross-section of the rhodolith with marked positions of the subsamples used for radiocarbon dating: (1) inner layer of calcareous red algae, (2) middle layer of calcareous red algae, (3) outer layer of encrusting red algae, (4) inner serpulid, and (5) outer serpulid. (**e**) and (**f**) Carbonate concretions from around 80 cm core depth.

Interquartile range (IQR) of postmortem ages of skeletal particles refers to time-averaging (mixing of non-contemporaneous generations, e.g. Tomašových and Kidwell 2010; Kidwell 2013). We assess (1) within-species time-averaging of 5 cm increments separately for *V. gibba* and *L. mediterraneum* and (2) multi-taxon time-averaging by assessing IQRs of all bivalves and rhodolith ages (with the exception of the few 5 cm increments where only one or two specimens of *L. mediterraneum* were dated).

Ten valves of *V. gibba* were randomly selected from five stratigraphic increments in the upper 30 cm of the core, where this species is abundant, and were dated by ^{14}C-calibrated amino acid racemization (AAR, Bada and McDonald 1995). We used the D/L of aspartic acid with the time-dependent reaction kinetic model and the initial D/L value estimated from data (TDK1; Allen *et al.* 2013). The calibration model is based on ^{14}C values of *V. gibba* shells collected in the Gulf of Trieste and the

parameters of the equation were given in Tomašových *et al.* (2017, 2018).

L. mediterraneum and rhodolith subsamples were dated by ^{14}C accelerator mass spectrometry (AMS) using the direct carbonate target technique (Bush *et al.* 2013). The rhodolith was cut and subsampled in zones that capture chronological succession of the rhodolith growing from its centre towards the outer parts: (1) inner layer of calcareous red algae, (2) middle layer of calcareous red algae, (3) outer layer of encrusting red algae, (4) inner serpulid, and (5) outer serpulid (Fig. 2d). All bivalves and rhodolith samples were prepared at the Amino Acid Geochronology Laboratory, Northern Arizona University (USA) and analysed at the Keck-Carbon Cycle AMS facility, University of California, Irvine (USA).

Two terrestrial plant remains were analysed by ^{14}C AMS at the Poznań radiocarbon laboratory (Poland) to date the sediments with low fossil content in the lower part of the core. All ^{14}C AMS data were calibrated using R version 4.0.3 (RCore-Team 2021) and package 'rcarbon' (Crema and Bevan 2021). Calibration of *L. mediterraneum* and rhodolith subsamples was based on the Marine20 calibration curve (Heaton *et al.* 2020), with regional marine reservoir correction (ΔR; i.e. regional offset from the marine ^{14}C calibration curve, Reimer and Reimer 2001) of -20 ± 28 years based on *Aequipecten opercularis* collected near Rimini (Langone *et al.* 1996). We note that $\Delta R = 139$ years in the marine13 database, as also used in Scarponi *et al.* (2013), changed to $\Delta R = -20$ years in the marine20 database. All ΔRs that were used to calibrate against the Marine13 databases in the past were updated in the 14CHRONO database of marine reservoir corrections (http://calib.org/marine/) so that they can be used with the marine20 database (Heaton *et al.* 2020). This shift does not prohibit the comparisons with former age calibrations, although more detailed analyses incorporating previously published ages may require recalibration of older geochronological data. Calibration for plant remains is following the atmospheric-based IntCal20 curve (Reimer *et al.* 2020).

Down-core profiles in ^{210}Pb

Activities of ^{210}Pb and ^{226}Ra were analysed in each core increment in the upper 60 cm by gamma spectrometry using a High Purity Germanium detector system at the Eawag Department Surface Waters (Switzerland). The excess in ^{210}Pb activity was computed by subtraction of ^{226}Ra from ^{210}Pb. As no apparent age homogeneity was visible in the uppermost centimetres, we computed apparent net sedimentation rates by fitting the slope of the activity decline in excess ^{210}Pb (with non-linear least-square fitting; with the excess ^{210}Pb activity declining exponentially with depth) according to the Constant Flux–Constant Sedimentation model (CFCS, Sanchez-Cabeza and Ruiz-Fernández 2012). In the absence of bioturbation, the slope of the log-linear decline in the excess ^{210}Pb activity is a function of sedimentation rate, with steeper slopes indicating faster sedimentation. If sedimentation rate is zero, the decline in the excess ^{210}Pb activity is a function of bioturbation. The excess ^{210}Pb activity is informative about sedimentation and mixing rate over the past one hundred years because the half-life of ^{210}Pb is 22.6 years.

Geochemistry

High-resolution sediment geochemistry is based on micro-X-ray fluorescence (μ-XRF) core scanning performed at the Austrian Core Facility (Institute of Geology, University of Innsbruck) on core halves. Sections were progressively moved past a No. 1 Mo-tube X-ray source of an Itrax-XRF core scanner (CS-45, Croudace and Rothwell 2015). The instrument was operated at 30 kV and 52 mA, with a count time of 5 seconds, and at 1000 μm sample resolution. Micro-XRF results are represented by counts per second (cps) and should be considered as semi-quantitative measurements.

The elemental intensities gained by the micro-XRF core scanning highlight stratigraphic variability in aragonite content (Sr), carbonate content (Ca), redox conditions (Fe, Mn), terrigenous input (Ti, K, Rb), grain size (Zr), and heavy metals (Pb, Zn, Cu, Ni) (Rothwell 2015). Molybdenum incoherent:coherent scattering ratio is a proxy for the content of organic matter (cf. Woodward and Gadd 2019).

Pairwise between-element comparisons were performed on selected element ratios. The decline in Ca/Sr, indicates a decline in biogenic aragonite content (Rothwell *et al.* 2006). Ti as a common constituent of rocks, such as gneiss or schist, indicates a terrigenous continental source (Rothwell *et al.* 2006). The ratio Ca/Ti increases with increasing contribution of carbonate at the expense of terrigenous components (Ingram *et al.* 2010). High ratio of Mn/Fe is indicative of reducing conditions in sediments (Marsh *et al.* 2007). We also plot Molybdenum incoherent scattering against Sr intensities to compare differences in organic matter content and aragonite content between facies units.

Bulk sediment geochemistry was analysed in 22 3 cm-thick subsamples to assess changes in major, minor and trace elements, nutrients, and persistent organic pollutants. Water content (WC) was determined from an aliquot of sample dried in an oven at 105°C until it reached a constant weight (Percival and Lindsay 1997). Total nitrogen (Ntot) and total

carbon (Ctot) were determined on subsamples using a ThermoFisher Flash 2000 IRMS Elemental Analyzer (EA). Samples for organic carbon (OC) were first decarbonated with hydrochlorid acid 1.5 N in silver capsules (Nieuwenhuize *et al.* 1994). Inorganic carbon (IC) was calculated as the difference between TC and OC. About 0.4 g of each sample dried at 55°C was digested with 8 ml of HNO_3 8 N in a microwave oven (USEPA 2007) and – after filtration – the concentrations of Al, As, Cr, Cu, Fe, Li, Mn, Ni, Pb and Zn were determined by ICP-AES spectrometry (Optima 2100DV, PerkinElmer, USA) (USEPA 1994). Mercury concentration was determined by cold-vapour AA spectrometry (Analyst 100, PerkinElmer, USA) (USEPA 1976). Raw concentrations of several trace elements in the bulk sediment were selected to quantify sediment pollution by comparing them to sediment toxicity criteria: effects range low (ERL) and effects range median (ERM) (Long *et al.* 1995; Burton *et al.* 2004). Concentrations below the ERL correlate rarely with toxic effects on benthic organisms, while concentrations above the ERM indicate generally or always observed toxic effects on benthic organisms. Trace elements were normalized to Fe in order to correct for grain size (Loring 1991; Covelli and Fontolan 1997; Covelli *et al.* 2006). Enrichment factors of grain-sizes, selected elements and components were calculated as the ratio between the mean concentrations in the upper 9 cm and the values averaged across the underlying intervals (Sucharovà *et al.* 2012).

Granulometry

The percentages of clay, silt, sand and gravel were determined in the same 3 cm-thick increments as used for bulk sediment geochemistry by a laser diffraction particle size analyser (Mastersizer 2000, Malvern Instruments Ltd 2007) using an aliquot of about 2 g of wet sediment dispersed in distilled water. The instrument provided the volumetric percentage of particles belonging to 100 diameter classes in the range 0.1 to 2000 µm. Grain-size classification followed Wentworth (1922).

Statistical analyses

All statistical analyses were performed in R 4.0.3 and RStudio version 1.4.1103 (RCoreTeam 2021; RStudioTeam 2021). Environmental variables (grain size and raw concentrations of nutrients and organic and inorganic pollutants) were checked for normality, log transformed when a non-normal distribution was detected, and z-standardized to account for different units and scales. Collinearity among geochemical variables was evaluated using the Pearson correlation coefficient and principal component

analysis (PCA) was used to assess multivariate relationships among samples with respect to their stratigraphic distribution. PCA was carried out based on a Euclidean distance, using the percentages of grain sizes (sand), and concentrations of major elements (Fe, Al, P, Mn), trace elements (As, Cd, Cr, Cu, Hg, Li, Ni, Pb, Zn), total nitrogen, total organic carbon, inorganic carbon, and organic pollutants (PAH). To identify the position of major stratigraphic shifts in bulk geochemistry and to agglomerate adjacent increments with similar composition into stratigraphic units, we used a constrained hierarchical cluster analysis that takes into account the stratigraphic sequence of the samples (Birks 2012). The clustering procedure is based on the CONISS algorithm applied to the Euclidean distance matrix (constrained incremental sum of squares agglomerative clustering, chclust function in the rioja package, Juggins 2015). This procedure links samples into successively larger groups by minimizing the Euclidean dispersion within the clusters, with the constraint that clusters must be formed by stratigraphically adjacent samples (Birks 2012).

Results

Facies 1: alluvial sandy silts (75–300 cm core depth)

The lowermost core section comprises light grey to beige sandy silts, mostly with a faint planar lamination (Fig. 3). Macrofauna is represented by sparse, non-marine molluscs such as the freshwater-brackish *Theodoxus* sp., *Valvata* sp., and *Pisidium* sp., along with land snails *Vallonia* sp. In total, nine non-marine poorly preserved molluscan remains were identified in this facies. Single valves of *V. gibba* occur at core depths 225 and 295 cm. Benthic foraminifers and ostracods are absent. Traces of bioturbation are almost absent apart from one preserved burrow at the base of the core, visible in the CT-scan (Fig. 3). Accumulation of well-preserved plant remains and wood fragments are frequent in this facies. Abundant millimetre-sized carbonate concretions occur at 75–100 cm (Fig. 2e, f).

Facies 2: transitional (coastal) sandy silts (40–75 cm)

This facies consists of grey sandy silts characterized by very low macro- and microfaunal densities, with maximum of *c.* 13 molluscs per 100 cm^3, *c.* 200 foraminifers per 1 cm^3, and *c.* 50 ostracods per 100 cm^3 (Fig. 3). The macrofossil assemblage comprises mostly a mixture of freshwater, brackish and marine molluscs (bivalves, gastropods, scaphopods and polyplacophors). Among 352 individuals that were
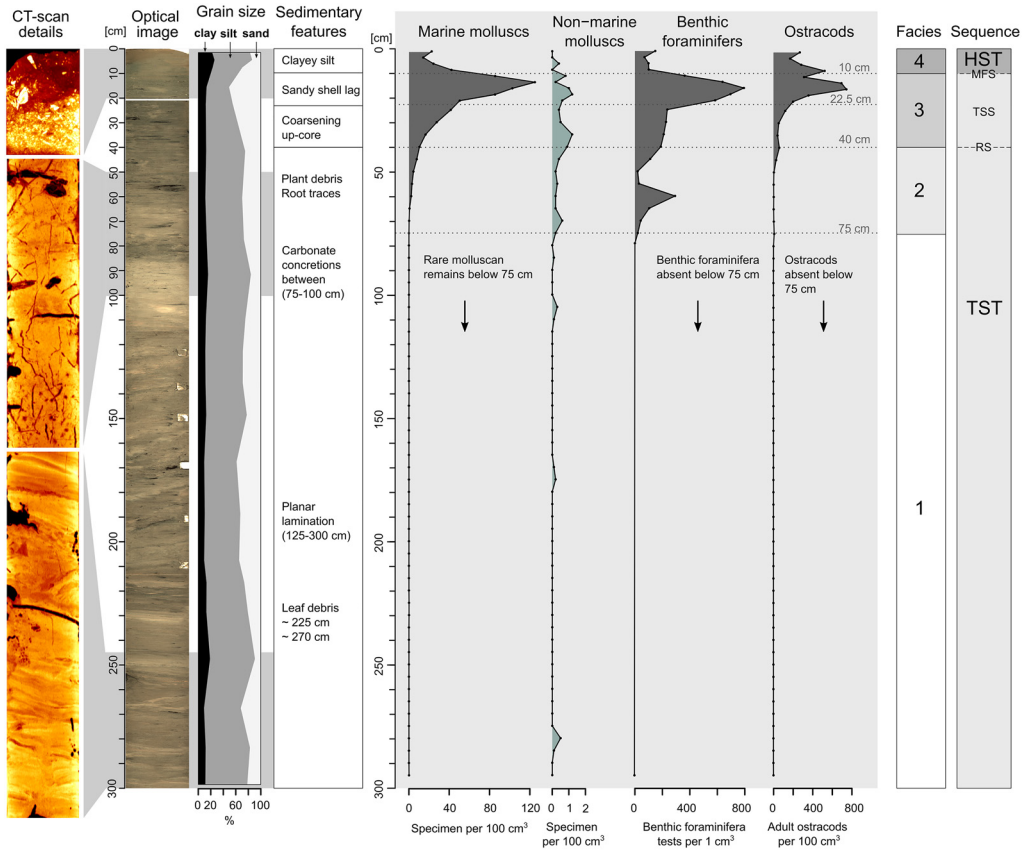
Fig. 3. POS514-GC25-5 core log. Left: Details of CT-scans visualizing sedimentary structures with lower (black to red) and higher (yellow to white) densities. Images are acquired with an X-ray penetration depth of 20 mm. Note that higher densities are indicated by lighter colours, for example in the shell lag around 10–20 cm and less dense material is indicated by black structures, for example by plant remains in the lower core segments. Optical images, grain sizes and core log with sedimentary structures are displayed. Centre: Faunal densities of marine and non-marine molluscs, benthic foraminifers and ostracods. Right: Facies and sequence stratigraphic interpretation of the core. The four facies include (1) alluvial/floodplain deposits, (2) transitional sediments, (3) a shallow-marine shell lag, and (4) prodelta silts. HST, highstand systems tract; TST, transgressive systems tract; MFS, maximum flooding surface; TSS, transgressive sand sheet; RS, ravinement surface.

identified to species level the dominant taxa are represented by marine bivalves: *V. gibba* (the most abundant mollusc, reaching up to 18%), *Parvicardium scabrum*, *Ostrea* spp., *Timoclea ovata*, *Pitar rudis*, *Nucula* cf. *nuclaeus*, and *Papillicardium papillosum* (Fig. 4). *Turritellinella tricarinata* is the most dominant marine gastropod (up to 10% of the total molluscan assemblage) (Fig. 4). Macrofauna is moderately- to poorly-preserved; most of the remains are fragmented, their original colour is absent, and external ornamentation is worn. The poorly preserved (highly abraded) microfauna is characterized by shallow-marine benthic foraminifers (*Haynesina* spp., *Ammonia* spp., *Textularia* spp.) and shallow-marine ostracods (*Cytheridea neapolitana*, *Loxoconcha* sp., *Cistacythereis* sp.)

(Fig. 4). Foraminifers peak in abundance at around 60 cm and ostracods appear for the first time above 50 cm (Figs 3 & 4). Few remains of freshwater-brackish species are represented by the gastropods *Vallonia* sp. and *Valvata* sp. and by the ostracod *Cyprideis torosa*. Plant remains and wood fragments occur occasionally; a prominent larger piece occurs at 55 cm core depth.

Facies 3: shallow-marine silty sands capped by a shell lag (10–40 cm)

This facies consists of grey silty sands that coarsen upward towards a shelly, densely packed lag in the uppermost 10 cm, with abundant micro- and

Human impacts in condensed shelf deposits
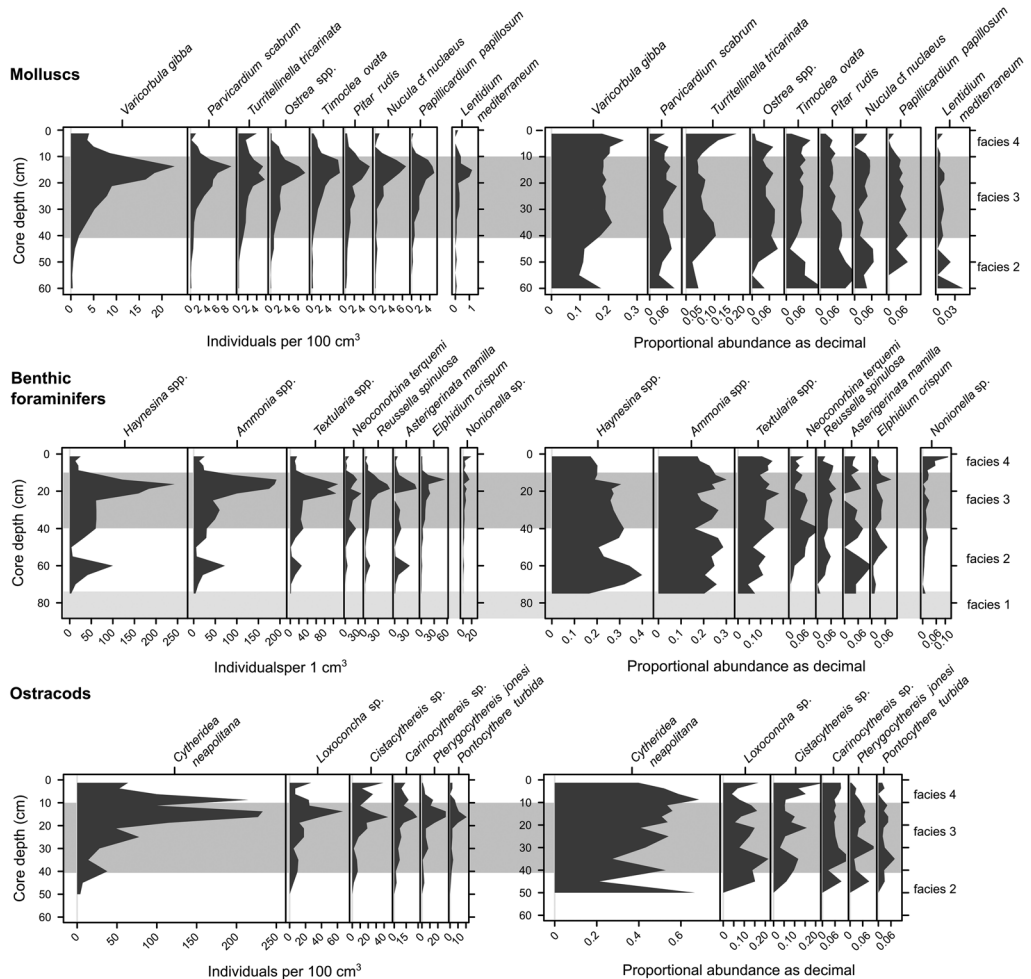
Fig. 4. Absolute and proportional abundance of the most common and index species. The sharp decline in absolute abundance at the transition from the shell lag to the uppermost 10 cm is driven by an increase in net sedimentation rate from *c.* 0.05 mm a^{-1} to 0.5 mm a^{-1}. The increase in proportional abundance of *Varicorbula gibba*, *Turritellinella tricarinata*. and *Nonionella* sp. in the uppermost 10 cm-thick prodelta silts is interpreted as a signature of eutrophication. Ostracods are represented by the most common species *Cytheridea neapolitana*. Note that total abundance of molluscs and ostracods below 60 and 45 cm drop below 10 individuals per increment due to a facies shift to alluvial deposits.

macrofossils. The macrofossil assemblage contains abundant fragments of bivalves and gastropods. Bryozoans, echinoderms, serpulids, crustaceans and otoliths are less common. The absolute abundance of molluscs reaches the maximum in the 12.5–15 cm increment with *c.* 120 specimens per 100 cm^3 (Fig. 3). In total, 3443 molluscs (bivalves, gastropods, scaphopods and polyplacophors) were identified in facies 3, among which 34 individuals belong to freshwater-brackish species (e.g. the gastropods *Vallonia* sp. and *Bithynia* sp.). The most dominant mollusc species is *V. gibba* (20%),

followed by the less abundant *P. scabrum*, *T. tricarinata*, *Ostrea* spp., *T. ovata*, *N.* cf. *nuclaeus*, and *P. papillosum* (Fig. 4). The preservation of macrofossils varies from worn fragments to well-preserved and complete larger shells. Most of the macrofossils are fragmented and externally discoloured. The shells often show traces of microborings and signs of internal dissolution. Some shells are partly coated by pyritic grains or encrusted. This facies is strongly bioturbated, with randomly oriented shells (see CT-scan in Fig. 3) and homogeneous median ages of *V. gibba* (Fig. 5).
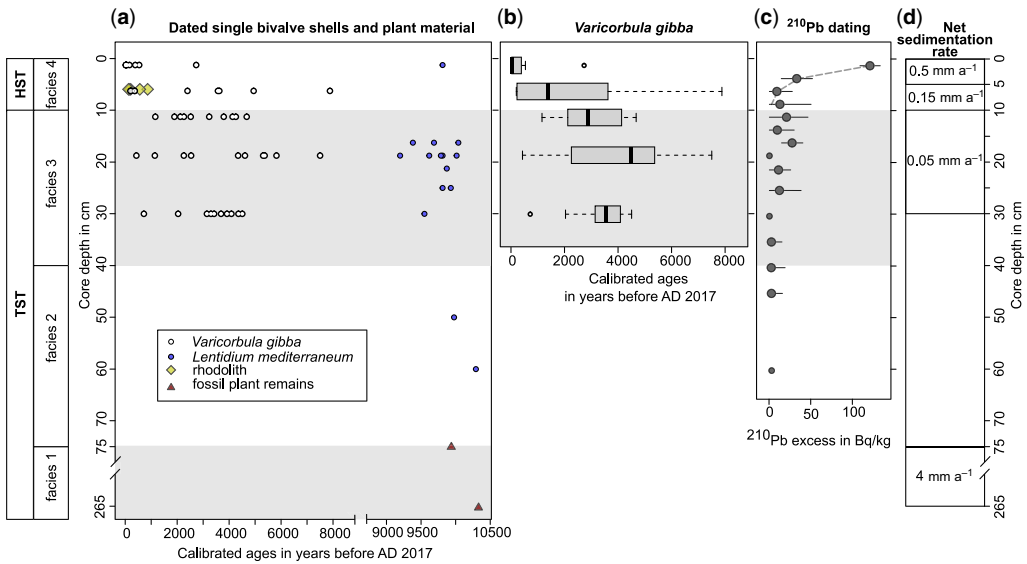
Fig. 5. (**a**) Calibrated radiometric ages of shells, rhodolith and plant remains in years before the year of core collection AD 2017. Postmortem ages of *Varicorbula gibba* are mostly younger than 7000 years, ranging from *c.* 24 to 7880 cal. years AD 2017. *Lentidium mediterraneum* ranges from *c.* 9200 to *c.* 10 290 cal. years AD 2017. The ages of the rhodolith subsamples range from 120 to 360 cal. years AD 2017, and plant remains are dated to *c.* 9938 and *c.* 10 400 cal. years AD 2017. (a–c) Grey backgrounds in the graphic highlight the different facies. (**b**) Distributions of *V. gibba* postmortem ages at their stratigraphic position visualized by boxplots that depict the first and the third quartile age and the median age of distributions. (**c**) ^{210}Pb excess in the sediments decreases in the upper 10 cm of the core down to background noise. (**d**) Calculated net sedimentation rate based on the dated shells.

The microfauna is poorly preserved (often abraded). Densities of shallow-marine benthic foraminifers (<300 specimens per 1 cm^3) and shallow-marine ostracods (<200 specimens per 100 cm^3) are low at the base of this facies (Fig. 3). Both foraminifers and ostracods show a rapid increase in densities at *c.* 20 cm core depth. The maximum densities of *c.* 800 foraminifera tests per 1 cm^3 and 750 adult ostracods per 100 cm^3 occur in the 15–17.5 cm increment. The dominant benthic foraminifers are represented by *Haynesina* spp., *Ammonia* spp., *Textularia* spp., *Neoconorbina terquemi*, *Reussella spinulosa*, *Asterigerinata mamilla*, and *Elphidium crispum* (Fig. 4). The ostracod assemblage is strongly dominated by *Cytheridea neapolitana* (50%) with other species (*Loxoconcha* sp., *Cistacythereis* sp., *Carinocythereis* sp., *Pterygocythereis jonesi*, and *Pontocythere turbida*) less frequent (Fig. 4).

Facies 4: prodelta silts (0–10 cm)

Clayey, fine to medium-grained, grey silts characterize the uppermost 10 cm of the core. The relatively low fossil content is mainly represented by marine molluscs (517 individuals in total), resulting in a mollusc density of 40 individuals per 100 cm^3. Non-

marine molluscs contribute only two individuals (Fig. 3). The molluscan assemblage shows an up-core decrease in absolute densities. This decline is exhibited by all dominant species, including *V. gibba*, *P. scabrum*, *T. tricarinata*, *Ostrea* spp., *T. ovata*, *P. rudis*, *N.* cf. *nuclaeus*, and *P. papillosum* (Fig. 4). However, proportional abundance of *T. tricarinata* (from *c.* 10% to *c.* 25%) and *V. gibba* (from *c.* 20% to *c.* 25%) increase up-core (Fig. 4). The fossil assemblage includes further a rhodolith (at 3–9 cm core depth, Fig. 2c, d) and several fragments of bryozoans, echinoderms, serpulids, crustaceans and otoliths. Skeletal remains are mostly fragmented, partly worn and discoloured. Periostracum is very rarely preserved on bivalve shells. Microbioerosion and mineral precipitation such as iron coatings and pyrite occur occasionally. The general homogeneity in grain sizes and random orientation of shells is a signature of mixing by bioturbation (CT-scan in Fig. 3), but differences in median ages of *V. gibba* (Fig. 5) indicate that this unit is not age-homogeneous and thus not fully mixed by burrowers. Size-frequency distributions of *V. gibba* show that the shell size increases in the uppermost 10 cm relative to the underlying shell lag (Fig. 6). The 95th percentile size increases from 5 to 6 mm to >9 mm in the top 10 cm, corresponding to higher
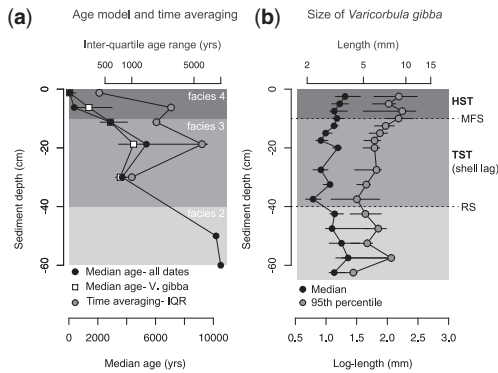
Fig. 6. (**a**) The down-core decline in median age of *V. gibba* (white boxes), in median ages of all dated skeletal remains (bivalves and rhodolith, black circles), and in interquartile age range based of all dated skeletal remains (grey circles). Grey background boxes indicate different facies. (**b**) Changes in the median shell length and in the 95th percentile length of *V. gibba* along the core indicating increase in size in the uppermost 10 cm. Grey background boxes correlate with different facies and HST (highstand systems tract) and TST (transgressive systems tract) and two surfaces are indicated: MFS (maximum flooding surface) and RS (ravinement surface).

frequency of shells >10 mm. The 95th percentile of the size distributions recorded in the six Van Veen grabs varies between 8.4 and 10.2 mm, documenting that the increase in size of *V. gibba* is not a patchy signal but is representative for the uppermost sediment centimetres penetrated by grabs.

The density of benthic foraminifers and ostracods declines strongly upwards, similarly to the marine molluscs (Fig. 3). Dominant benthic foraminifers are represented by *Haynesina* spp., *Ammonia* spp., *Textularia* spp., *Neoconorbina terquemi*, *Reussella spinulosa*, *Asterigerinata mamilla*, and *Elphidium crispum* (Fig. 4). The proportional abundances of these species show a strong decrease towards the top of this facies unit. In contrast, *Nonionella* sp. increases upwards, reaching 10% of the total foraminiferal assemblage. The shallow-marine ostracods are dominated by a single species, *Cytheridea neapolitana* (70%) (Fig. 4). Other marine ostracod species such as *Loxoconcha* sp. and *Cistacythereis* sp. contribute less than 20% each to the fossil assemblage. *Carinocythereis* sp., *Pterygocythereis jonesi*, and *Pontocythere turbida* are less abundant than 10% each; Fig. 4).

Core chronology

Radiocarbon dates of two terrestrial plant macrofossils at 75 and 265 cm show that the alluvial sandy silts (facies 1) in the lower part of the core were

deposited between *c.* 9940 and *c.* 10 400 cal years AD2017 (Fig. 5a, Table 1). Notably, ages of *L. mediterraneum* collected from the overlying increments in the upper 60 cm of core (facies 2–4) show a similar range (Fig. 2b). Ages of *L. mediterraneum*, sampled in the upper 60 cm of the core, do not vary systematically with the stratigraphic position, ranging between 9380 and 10 510 cal years AD2017 (Fig. 5a). In contrast, ages of *V. gibba* (Fig. 2a) are younger by several millennia and range from 24 to 7880 cal years AD2017, with most of them being younger than *c.* 5000 years (Fig. 5a). Only two shells of *V. gibba* are older than 7000 years (Fig. 5a). The total age range of *L. mediterraneum* in the entire core is 1130 years and IQR is 310 years. Whole-core total age range and IQR of *V. gibba* are both higher by an order of magnitude (7860 years and 3720 years, respectively). Moreover, in contrast to *L. mediterraneum*, median ages of *V. gibba* show a stratigraphic order within the uppermost 30 cm of the core (Fig. 5b). Median age of *V. gibba* increases down-core from 50 years at 0–2.5 cm, to 1380 years at 5–7.5 cm, to *c.* 2880 years at 10–12.5 cm, to 4480 years at 17.5–20 cm, and reverses to 3560 years at 27.5–32.5 cm (Fig. 5b). The age distribution of *V. gibba* at 5–7.5 cm, representing the transition between the top-core increment with very young shells and the underlying shell lag with shells that are several millennia old, is in fact characterized by two distinct modes – five shells are between *c.* 200 and 370 years old and five shells are between *c.* 2400 and *c.* 7900 years. The rhodolith found at 3–9 cm was formed by several organisms, mainly by coralline red algae, serpulids, encrusting red algae, and bryozoans (Fig. 2c, d). Age dating of 5 subsamples show that the rhodolithic innermost segments grew from 500 to 270 cal years AD2017. These inner layers were overgrown by serpulids in 190 and 200 cal years AD2017. The rhodolith thus grew gradually over the duration of at least 300 years until the *c.* nineteenth century (Fig. 5a) and is coeval with the subset of shells of *V. gibba* at 5–7.5 cm (200–400 years old). The overall age model for the upper 60 cm of the core based on ages of all skeletal particles (*V. gibba*, *L. mediterraneum*, and five rhodolith subsamples) shows a down-core increase in per-increment median age up to *c.* 4480 years at 20 cm, followed by the reversal to *c.* 3560 years at 30 cm (Fig. 6). *L. mediterraneum* at 50–60 cm constrains the onset of the facies 3 to *c.* 10 000 years (Fig. 6).

Time-averaging

Per-increment time-averaging of *V. gibba* as measured by the IQR increases rapidly down-core from 300 years at 0–2.5 cm to 3350 years at 5–7.5 cm. The increments in the shell lag (facies 2) show IQR

Table 1. *Facies interpretation*

Facies	Core depth (cm)	Lithology	Age dating	Sedimentation rate	Sequence
facies 4: prodelta sediments	0–10	muddy silt	0–2.5 cm increment: *c.* 50 years before AD 2017 based on *V. gibba* median shell ages	increasing up-core, *c.* 0.5 mm a^{-1} in the top based on Pb dating, 0.15 mm a^{-1} at the bottom based on *V. gibba* shell dating	HST
facies 3: shallow-marine sediments	10–40	muddy/silty sand including a shell-rich lag (10–22.5 cm)	*c.* 2000–7800 years before AD 2017 based on *V. gibba* shell dating	*c.* 0.05 mm a^{-1} based on *V. gibba* shell dating	TST
facies 2: transitional (coastal) sediments	40–75	sandy silts	<*c.* 9940 ($\pm$50 years) before AD 2017 based on dated plant remains	decreasing up-core, *c.* 4 mm a^{-1} based on dated plant remains	TST
facies 1: alluvial sediments	75–300	sandy silts	*c.* 9940–10 400 ($\pm$50 years) before AD 2017 based on dated plant remains	*c.* 4 mm a^{-1} based on dated plant remains	TST

Ages and estimates of the net sedimentation rate are based on different faunal materials and plant remains.

of 1890 years at 10–12.5 cm, 3030 years at 17.5–20 cm, and 860 years at 27.5–32.5 cm. IQRs based on ages of all skeletal particles parallel the trends exhibited by IQRs of *V. gibba* ages, markedly increasing from 430 years at 0–2.5 cm to 2760 years at 5–7.5 cm, with millennial-scale IQRs below (Fig. 6a).
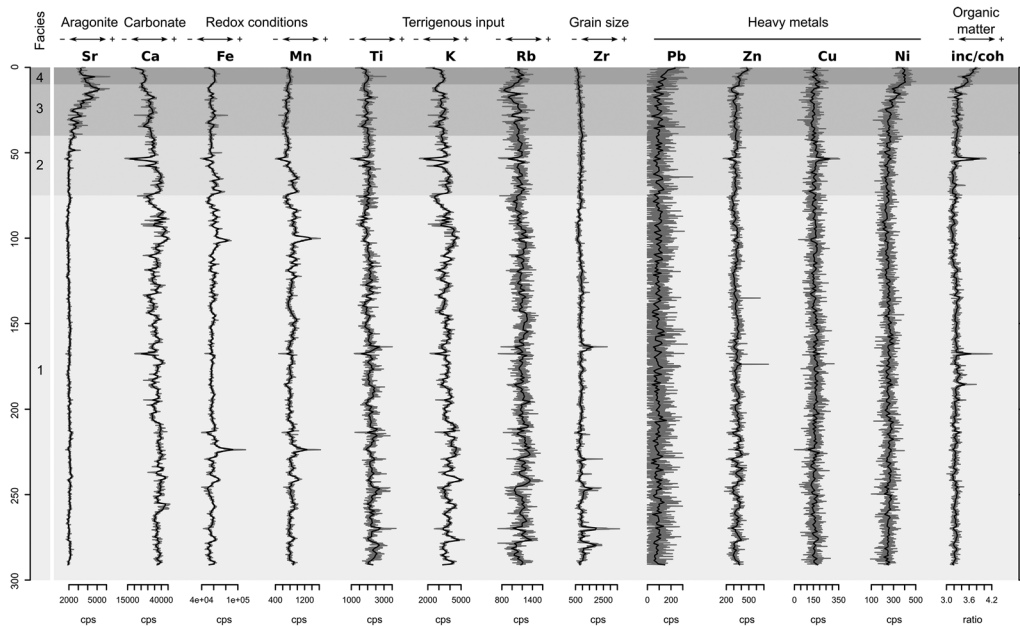
Fig. 7. Micro-XRF core scanning in 1 mm resolution (grey lines) and averaged to 10 mm signals (black lines). All single element intensities in counts per second (cps).

Sedimentation rates

Based on all ages of carbonate skeletal particles (both bivalve species and the rhodolith), the uppermost 2.5 cm increment with median age equal to *c.* 50 years was deposited at 0.5 mm a^{-1} during the twentieth century (i.e. 50 years/25 mm, Fig. 5a, b). The difference in median ages between the increment at 0–2.5 cm and at 5–7.5 cm (including the rhodolith dates) shows that sediments were deposited at 0.15 mm a^{-1} over few centuries prior to the twentieth century. The non-linear least squares regression fitted to the exponentially-declining excess ^{210}Pb activity in the uppermost core segment (0–10 cm) documents an apparent net sedimentation rate of 0.6 mm a^{-1} during the twentieth century (Fig. 8c), similar to the estimate based on median ^{14}C ages of skeletal particles in the uppermost increment (0–2.5 cm, Fig. 8b).

The differences in *V. gibba* median age between increments corresponding to the shell lag (i.e. the difference in median ages between increments at 5–7.5 cm and 10–12.5 cm, or between 10 and 12.5 and 17.5–20 cm, divided by the corresponding depth differences) documents a net sedimentation rate of *c.* 0.02–0.05 mm a^{-1} during the Late Holocene sea-level rise between *c.* 1000 and 6000 years ago as suggested by ages of shells in facies 3. In contrast, the age difference of only 450 years between the dated plant remains suggests a high net sedimentation rate of *c.* 4 mm a^{-1} during the deposition of alluvial floodplain (TST) sediments preserved now at 75–265 cm (Fig. 8d, Table 1).

## High-resolution sediment geochemistry

Although all element intensities from micro-XRF fluctuate within the core, directional stratigraphic changes were observed only in a few cases (Fig. 8). Aragonite content tracked by Sr shows low, stable intensities in facies 1 and 2, and a gradual up-core increase to a maximum in facies 3 at *c.* 12 cm (Fig. 7). Carbonate content tracked by Ca intensities remains constant throughout the core. At around 55 cm (facies 2), a centimetre-sized plant remain induced the negative excursions of Ca, Ti and K and the positive Molybdenum incoherent: coherent scattering ratio. Fe and Mn intensities are lowest in facies 2, and do not change markedly in the upper 1 m of the core. The intensity of K (terrigenous input) decreases at the top of facies 1, where the carbonate concretions occur, and at the top of facies 3 (within the shell lag). Higher Zr intensities indicate coarser grained sediments in a few horizons at the base of the core. The concentrations of Pb, Zn and Ni increase slightly in the topmost increments. Between-element pairwise plots show that the lower core parts (facies 1) are characterized by high Ca and low Sr intensities (Fig. 9). Ca slightly decreases within facies 2, while Sr increases until it reaches its maximum in facies 4. Molybdenum incoherent:coherent scattering ratio shows a broader range and lower intensities in facies 1 and 2 than in facies 3 and 4. Ti attains the highest values in facies 1 and decreases up-core.

Bulk sediment geochemistry

Quantitative geochemical analyses of bulk sediment led to the identification of stratigraphic shifts in the concentrations of trace elements, major constituents (mainly clay minerals) and pollutants (Fig. 9). Remarkably, these concentrations are not significantly changing at the transition from alluvial to marine sediments at *c.* 22.5–75 cm (facies 1 to 3). In contrast, a prominent excursion is visible in Hg, Cr, Ni, Pb, Li, and Al in the uppermost 9 cm (facies 4, Fig. 9). Concentrations of Cu, Cd and Mn markedly decrease in facies 3 at 15 cm. Zn, Pb and Cr fall below the ERL, while Hg concentrations exceed the ERL benchmarks in the upper 9 cm. Ni concentrations exceed the ERL in the upper 75 cm and almost reach the ERM in the uppermost 10 cm. The concentrations of As exceed the ERL benchmark at several intervals, but remain below ERM (70 mg kg^{-1}). The proportion of fine-grained fraction (<16 μm), total nitrogen, TOC and water content increase up-core within the HST units (Fig. 9). The concentrations of P and Fe decrease in facies 3 at 15 cm, but do not increase in the overlying facies 4. The lower core segments exhibit low organic enrichment, but TOC increases strongly in the uppermost 10 cm. The carbonate content based on IC ranges from 33 to 42% and has its maximum at 85 cm, where carbonate concretions are frequent. Up-core, the carbonate content decreases gradually to a minimum of 26% at 7.5 cm (Fig. 9). Enrichment factors show that total nitrogen and organic carbon increase by a factor of 3.7 and 2.3, respectively, towards the uppermost core segment (Table 2). The amount of P does not increase upwards. The concentration of Hg shows a drastic increase (7.4); Pb, Cr, Ni and Zn also show an up-core increase (EF 2.3–1.5). Percentage of sand-sized grains correlates positively with concentrations of As (Table 3). Silt correlates positively with Fe, C_{tot}, Mn and Cu. Fine-grained fraction (<16 μm) correlates positively with the concentrations of Ni, Hg, Cr, Pb, Li, Al, Zn and total nitrogen.

Constrained hierarchical cluster analysis based on bulk geochemistry discriminates two main groups, corresponding to facies 1–3 (9–300 cm) and facies 4 (0–9 cm) (Fig. 10), suggesting a major change in bulk geochemistry at the transition between the shell lag and the prodelta silts.
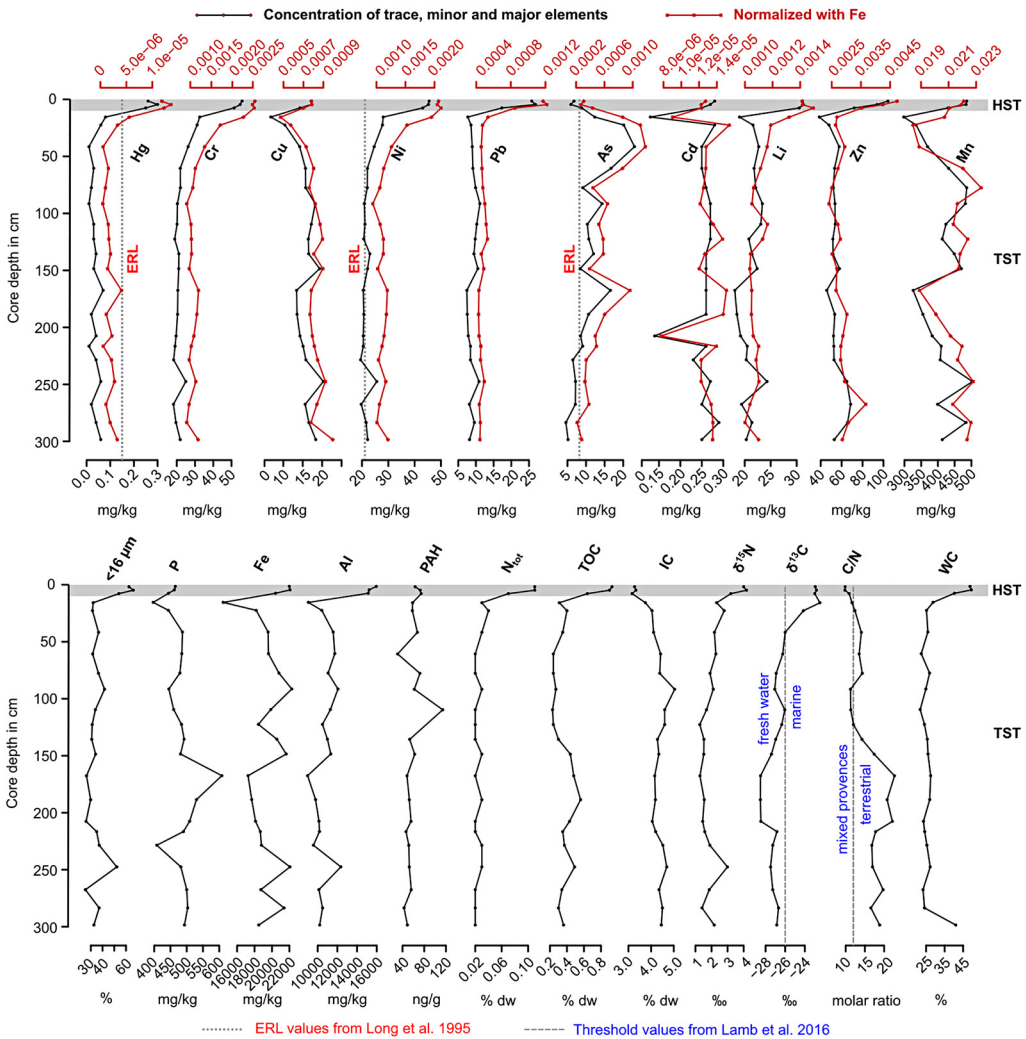
Fig. 8. Trace elements, major constituents and organic components from bulk geochemistry. Trace elements are normalized with Fe to avoid grain size effects (grey lines). Effect Range Low (ERL) threshold values from Long *et al.* (1995) are marked with a dashed line. Thresholds for carbon isotopes ($\Delta^{13}C$) and carbon to nitrogen ratio (C/N) as palaeoproxies follow Lamb *et al.* (2006).

Increment at 15.5 cm is separated from all underlying samples. The lower part of the core is further divided at *c.* 160 cm into two groups of increments, which, however, are less clearly separated and not supported by the results of the PCA based on the same data. PCA illustrates the correlation between elements, with the first two axes explaining 72% of the variance in the data (Fig. 10). This approach distinguishes two major groups of samples differing in grain size and geochemical composition. Group 1, identified by the cluster analysis, comprises organic-rich, fine-grained sediments with heavy metal pollutants Pb, Hg and Ni in the upper 9 cm

of the core (increments 1.5, 4.5 and 7.5 cm). Group 2 comprises most of the remaining increments arranged along a gradient from sandy sediments with high concentrations of As (increments at 22.5, 41.5, 167.5, 188.5, and 207.5 cm) to silt-dominated sediments with high carbonate content and high concentrations of Fe, P, Mn, and Cd (increments between 77.5–148.5 cm and 216.5–298.5 cm). The increment at 15.5 cm is an outlier both in the cluster analysis and in the PCA. This increment corresponds to the sandy shell lag with the highest proportion of sand in the entire core and with the maximum densities of skeletal remains (Figs 3 & 4).
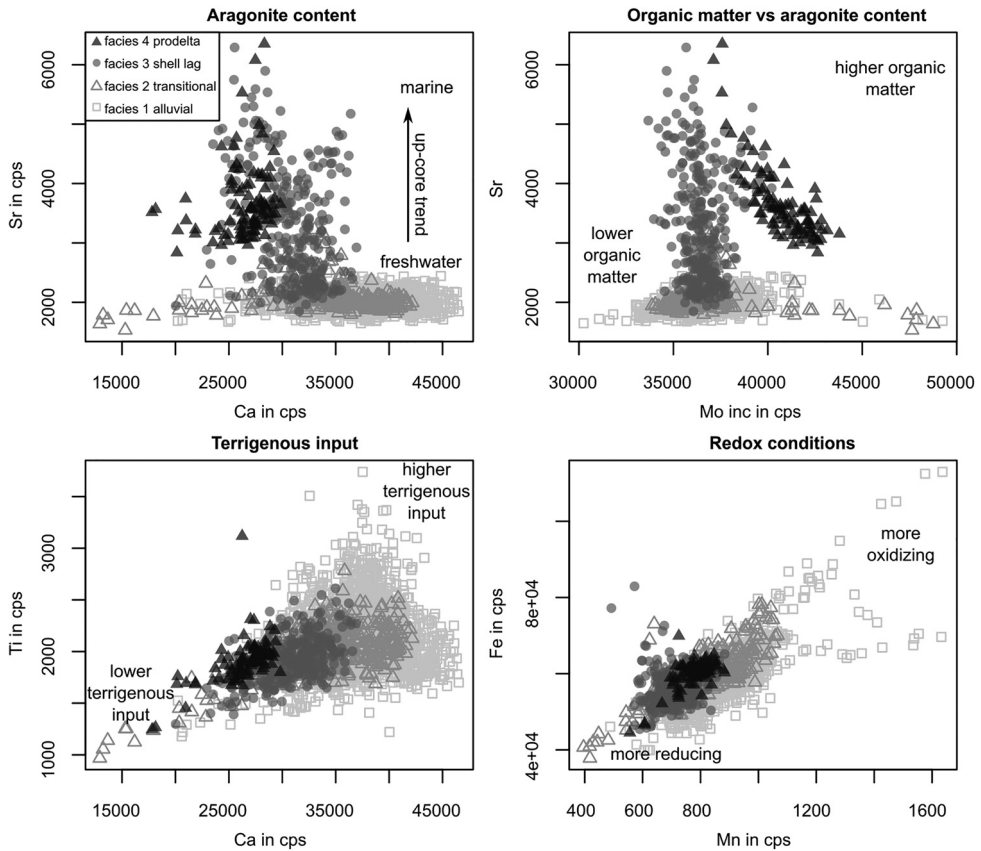
Fig. 9. Bivariate relationships between element concentrations that represent indicators of aragonite content, organic matter, terrigenous input and redox conditions, based on micro-XRF element ratios: Ca/Sr, Mo inc/Sr, Ca/Ti, Mn/Fe.

Discussion

Facies interpretation, sequence stratigraphy and palaeoenvironmental conditions

Four facies are expressed in the stratigraphic record of the 300 cm long gravity core (Table 1). Although the alluvial sediments were deposited under relatively high net sedimentation rates, the marine succession preserved in the 70 cm-thick section is extremely condensed.

Facies 1: alluvial floodplain (75–300 cm)

Sediment features and fossil content indicate that facies 1 was deposited in an alluvial floodplain setting. The widespread presence of plant debris, the millimetre-scale lamination and geochemical proxies (Fig. 8) indicate a setting with low topography affected by recurrent floods. Abundant carbonate concretions at the top of the facies probably represent coatings and filaments precipitated along root traces

(i.e. root casts, Fig. 2e, f). These concretions indicate water level oscillations and carbonate supersaturation of sediment pore-waters. They can be interpreted as early pedogenic features similar to those described by Amorosi et al. (2021) from soil horizons in Po plain deposits. The depositional setting of facies 1 can thus be assigned to a poorly-drained floodplain (*sensu* Amorosi et al. 2017) indicated by (1) the paucity of *in situ* and reworked macrobenthic remains, (2) single occurrences of diagnostic taxa (e.g. the freshwater-brackish bivalve *Pisidium* sp.), (3) the absence of microfauna, and (4) the occurrence of carbonate concretions. Two occurrences of *V. gibba* are interpreted as out-of-habitat transport. Facies 1 has similarities with the poorly-drained floodplain facies association formed as part of an inner estuary depositional system of Amorosi et al. (2017) documented in the Holocene transgressive systems tract of the Po plain. The sedimentation rate of *c.* 4 mm a^{-1} (Table 1) is likely an estimate that averages episodes of high sedimentation and episodes of exhumation or non-deposition as is

Table 2. *Enrichment factors (EF) based on bulk geochemistry results in the 3 upper layers (0–9 cm)*

	As	Sand	IC	Ctot	Silt	P	Cu	Cd	Fe	Mn	PAH	Al	Li	Zn	WC	Clay	Ni	OC	Cr	Pb	N_{tot}	AH	Hg
EF	0.6	0.7	0.7	0.9	0.9	0.9	1.1	1.1	1.1	1.1	1.2	1.5	1.5	1.7	1.8	1.9	2	2.3	2.5	2.6	3.7	4.4	7.4

Background values are based on the underlying intervals (15–300 cm). Heavy metals were normalized to the Fe content.

typical of floodplain deposition. The timing of the deposition of facies 1 at *c.* 10 000 years ago is coeval with a phase of a step-wise, but rapid sea-level rise in the Northern Adriatic Sea (Lambeck *et al.* 2014; Amorosi *et al.* 2017). This facies thus corresponds to the TST units that belong to a landward-thickening transgressive sediment wedge in cores and seismic profiles in this sector of the Northern Adriatic Sea (Correggiari *et al.* 1996b; Storms *et al.* 2008). Floodplain deposits that characterized the NW Adriatic environments during the first phases of sea-level rise prior to *c.* 11 000 years (Picone *et al.* 2008), were typically replaced by barrier-lagoon sediments that rimmed the retrograding shoreline during the later phases of the TST, with high lateral variability in water depth. Large parts of the flat northern Adriatic shelf were flooded during the subsequent *c.* 500 years when the global sea level rose by *c.* 6.5 m. However, the sampling position was still *c.* 25 km away from the shoreline (Fig. 11; Lambeck *et al.* 2014).

Facies 2: transitional coastal sediments (40–75 cm)

Based on fossil content and sediment features, facies 2 comprises transitional coastal sediments, with similarities to the underlying floodplain facies (regarding grain-size and organic matter remains) and to the overlying shallow-marine sediments (e.g. gradually increasing macro- and microfossil content) (Fig. 3). On one hand, the abundance of ostracods and molluscs is very low in this facies, indicating conditions reflecting the deposition in restricted coastal lagoons. On the other hand, the increasing abundance of marine fauna including *V. gibba* indicates an offshore-transitional settings with water depths >10 m (Hrs-Brenko 2006). The macrofossil assemblage consists of rare freshwater-brackish fauna, suggesting reworking and/or out-of-habitat transport (Fig. 3). The absolute abundance of foraminifers increases rapidly at 60 cm, followed by a drop to low abundances, while the ostracod assemblage shows very low abundances throughout facies 2 (Fig. 3). These co-occurrence patterns indicate mixture of alluvial and shallow-marine sediments. The transitional character of this facies is reflected in the geochemical profiles as well: (1) a gradual increase in the contribution of biogenic aragonite, (Fig. 7), (2) a gradual shift towards more positive $\delta^{13}C$ of organic matter, indicating an increase in contribution of marine organic matter (Lamb *et al.* 2006) (Fig. 8), and (3) a decrease in C/N values (mixing of marine and terrestrial organic matter) (Lamb *et al.* 2006, Fig. 8). Major and trace elements are not changing significantly along facies 2, indicating a constant source of terrestrial input (Fig. 8). To

**Table 3.** *Pairwise Pearson correlation coefficient values for bulk geochemistry and grain size*

	Hg	Cr	Cu	Ni	Pb	As	Cd	Li	Zn	Mn	P	Fe	Al	<16 μm	Sand	PAH	N_{tot}	OC	IC	WC
Cr	**0.96**																			
Cu	0.03	−0.09																		
Ni	**0.97**	**1**	−0.03																	
Pb	**0.91**	**0.89**	0.27	**0.91**																
As	−0.29	−0.12	**−0.46**	−0.17	−0.32															
Cd	0.11	0.08	**0.55**	0.12	0.28	−0.02														
Li	**0.86**	**0.88**	0.33	**0.9**	**0.93**	−0.22	0.34													
Zn	**0.79**	**0.76**	0.41	**0.78**	**0.91**	**−0.43**	0.37	**0.84**												
Mn	0.25	0.19	**0.84**	0.25	**0.51**	**−0.52**	**0.5**	**0.58**	**0.57**											
P	−0.22	−0.33	0.16	−0.32	−0.23	0.1	0.22	−0.34	−0.08	−0.11										
Fe	0.3	0.28	**0.8**	0.34	**0.56**	−0.28	**0.61**	**0.67**	0.63	**0.93**	−0.06									
Al	**0.82**	**0.84**	0.38	**0.87**	**0.91**	−0.19	0.35	**0.98**	**0.85**	**0.61**	−0.26	**0.7**								
<16 μm	**0.83**	**0.83**	0.34	**0.86**	**0.91**	−0.33	0.3	**0.93**	**0.83**	**0.59**	−0.35	**0.64**	**0.9**							
Sand	−0.21	−0.13	**−0.89**	−0.19	**−0.46**	**0.48**	**−0.51**	**−0.51**	**−0.58**	**−0.86**	0.05	**−0.85**	**−0.53**	**−0.61**						
PAH	0.25	0.3	0.02	0.29	0.27	−0.02	−0.01	0.37	0.21	0.11	−0.24	0.23	0.32	0.28	−0.1					
N_{tot}	**0.95**	**0.95**	0.08	**0.95**	**0.96**	−0.23	0.19	**0.88**	**0.86**	0.3	−0.23	0.39	**0.85**	**0.87**	−0.3	0.26				
OC	**0.87**	**0.84**	0.1	**0.84**	**0.84**	−0.28	0.14	**0.72**	**0.81**	0.19	0.02	0.3	**0.71**	**0.76**	−0.27	0.2	**0.92**			
IC	**−0.84**	**−0.87**	0.38	**−0.85**	**−0.67**	0.07	0.17	**−0.6**	**−0.56**	0.14	0.14	0.07	**−0.57**	**-0.53**	−0.21	−0.24	**−0.78**	**−0.77**		
C/N	**−0.49**	**−0.6**	0.02	**−0.61**	**−0.59**	−0.13	−0.22	**−0.68**	−0.36	−0.31	**0.69**	−0.34	**−0.63**	**−0.59**	0.16	−0.25	**−0.53**	−0.17	0.3	
WC	**0.9**	**0.86**	0.14	**0.87**	**0.84**	-0.36	0.14	**0.76**	**0.75**	0.27	-0.15	0.29	**0.73**	**0.78**	−0.31	0.19	**0.88**	**0.83**	**−0.72**	−0.37

Significant correlations ($p < 0.05$) are displayed in bold.

Human impacts in condensed shelf deposits
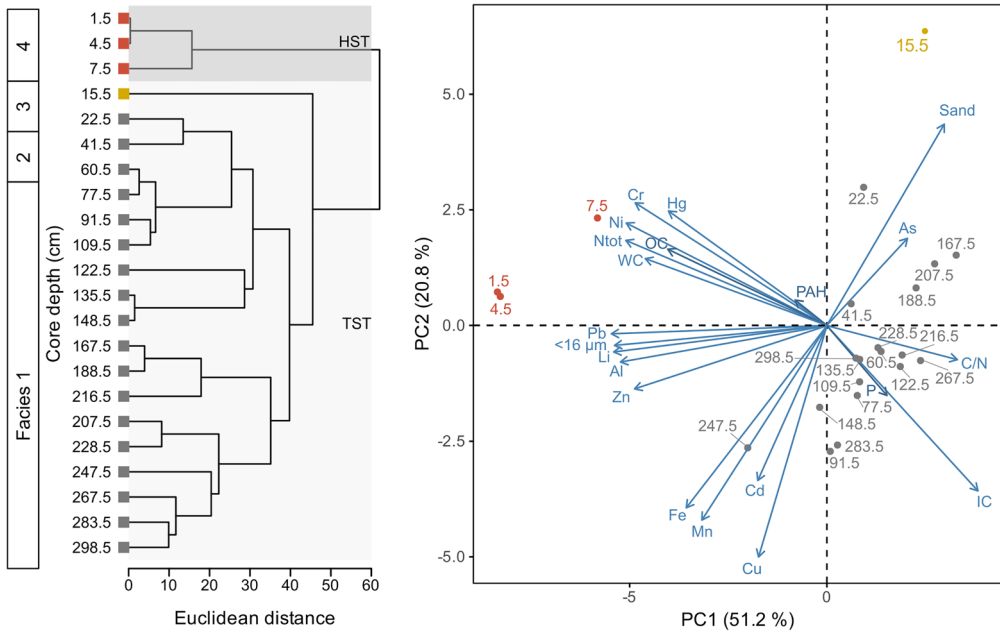
Fig. 10. Constrained cluster analysis and principal component analysis of selected bulk geochemical data. Variables were log-transformed and normalized to z-scores beforehand. Both analyses are based on Euclidean distances.
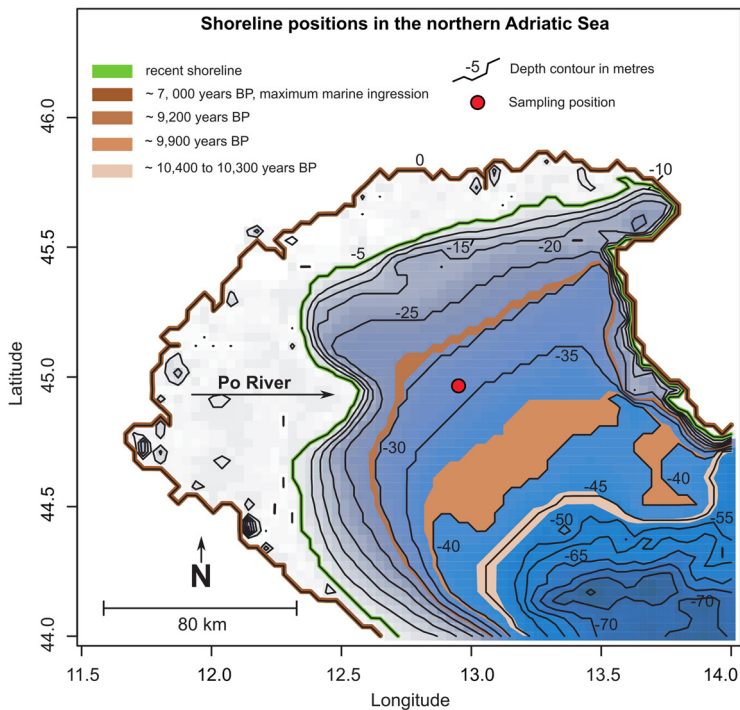
Fig. 11. Development of shorelines in the Northern Adriatic Sea based on the global sea-level curve of Lambeck *et al.* (2014). The Recent shoreline is at −5 m due to subsidence. Maximum marine ingression based on Correggiari *et al.* (1996*b*).

conclude, facies 2 marks the transition from alluvial/floodplain to shallow-marine setting in a transgressive systems tract and shows similarities to transgressive deposits from Holocene sediment cores from the Po plain described by Amorosi *et al.* (2017).

Facies 3: transgressive sand sheet with shell lag (10–40 cm)

Facies 3 is expressed by a conspicuous shell lag dominated by marine mollusc shells (bivalves and gastropods) with other marine organisms (bryozoans, echinoderms, serpulids, and crustaceans). A similar shell lag located close to the present-day sediment–water interface is a typical feature of Holocene successions in the central segments of the Northern Adriatic Sea (Picone *et al.* 2008). *V. gibba* dominating the fossil assemblage indicates that the water depth exceeded 10 m (Hrs-Brenko 2006) (Figs 3 & 4). Subtidal conditions buffered from salinity or temperature fluctuations led to the development of diverse micro- and macrofaunal communities (Figs 3 & 4). Rare brackish-freshwater molluscs in the fossil assemblage are reworked or transported from marginal marine (*L. mediterraneum*) or fresh-water habitats (*Pisidium* sp.). Although the contribution of freshwater-brackish fauna is significantly lower than the contribution of marine fauna, (1) the co-occurrence of environmentally non-overlapping taxa, (2) millennial-scale time-averaging of skeletal remains, and (3) poor skeletal preservation demonstrate environmental condensation of benthic communities (e.g. Fürsich 1978; Kidwell 1998, 2013) (Fig. 3). The shell lag exhibits signs of taphonomic feedback (Kidwell 1986) as suggested by colonization of dead shells by encrusting bryozoans, encrusting red algae and serpulids. Shell preservation in this facies is linked to (1) low net sedimentation rates that were probably on the long term induced by longshore currents and/or by episodic winnowing of fines by storms (*c.* 0.05 mm a^{-1}) and (2) deep bioturbation promoted by infaunal organisms as indicated by age-homogeneity of *V. gibba* across 20 cm and by even higher vertical spread of *L. mediterraneum* (Fig. 5). Age data indicate that the formation of the shell lag coincides with the development of counterclockwise bottom currents that likely increased sediment winnowing and bypassing. These bottom currents in the Northern Adriatic Sea became stronger *c.* 7000–7700 years ago, when the circulation intensified in response to the sea-level rise (Lambeck *et al.* 2014) and the shoreline achieved the most landward position (Amorosi *et al.* 2017). This period corresponds to the maximum age of *V. gibba* from our core material (Fig. 5). The lithology, fossil content and age data thus indicate that facies 3 with the shell lag can be assigned to a transgressive sand sheet (sensu Amorosi *et al.* 2017; Scarponi *et al.* 2017), which is a thin, shell-rich stratigraphic interval with strong evidence of reworking by coastal processes during shore-face retreat. In the sequence stratigraphic architecture of the Northern Adriatic Sea, the transgressive sand sheet is typically bounded by the wave ravinement surface at the base (an erosional surface produced by shelf currents and/or waves) and by the maximum flooding surface at the top (marking the change from maximum shoreline migration to early Po delta progradation) (Amorosi *et al.* 2017; Scarponi *et al.* 2017; Zecchin *et al.* 2019). However, in the studied core the base of the shell lag does not exhibit a clear erosional surface. The lack of well-developed ravinement surface may indicate that (1) the transgressing shoreline environment at the location of our core was characterized by a low-energy regime, without significant waves or tides in the shore-zone (Cattaneo and Steel 2003), or (2) that the erosional surface was initially present but was subsequently erased by deep bioturbation during deposition of the shell lag. In the latter scenario, the wave-ravinement surface is interpreted to be originally located below a conspicuous increase in abundance of skeletal remains at 40 cm, separating shallow-marine deposits from the mixed floodplain-coastal to marine deposits.

Facies 4: prodelta silts (0–10 cm)

Facies 4 is formed by clayey silts containing dead shells that are actively sourced from the present-day benthic community. It can be assigned to the distal prodelta facies association of Amorosi *et al.* (2017) as suggested by (1) the high proportion of taxa that inhabit such settings (e.g. *V. gibba*, *T. tricarinata*, *Nonionella* sp., Fig. 4), (2) terrigenous input driven by river-borne sediment (mainly coming from the Po della Pila mouth of Po River), and (3) the present-day depositional setting below fair weather wave base at 31 m water depth. Three key species increase in proportional abundance in facies 4: the benthic foraminifer *Nonionella* sp. (from *c.* 1% to *c.* 10% per increment), the opportunistic bivalve *V. gibba* (from *c.* 20% to *c.* 25% per increment), and the gastropod *T. tricarinata* (from *c.* 5% to *c.* 15% per increment, reported as *Turritella communis* in Vatova 1949) (Fig. 4). *V. gibba* increases in median and maximum size in prodelta silts relative to its size in the underlying shell lag (Fig. 6). The ostracod species *Cytheridea neapolitana* decreases in proportional abundance up-core, while less abundant species such as *Loxoconcha* sp. increase (Fig. 4). All these species prefer a distal prodelta/mud-belt environment with organic-rich sediments (Rossi and Vaiani 2008; Barbieri *et al.* 2019). *Nonionella* sp. and *V. gibba* can tolerate oxygen-depleted conditions and thus can benefit from the eutrophication

directly (higher food supply) and indirectly when hypoxic episodes intensified by the eutrophication eliminate their competitors or predators (Van der Zwaan and Jorissen 1991; Hrs-Brenko 2006; Barbieri *et al.* 2019) Suspension-feeding turritelline gastropods also benefit from high primary productivity resulting from eutrophication (Allmon 2011). However, *T. tricarinata* is rather sensitive to oxygen depletion (Crema *et al.* 1991; Chiantore *et al.* 2001).

Sediment cores collected at sites with higher stratigraphic resolution show that the abundance of *Nonionella* increased in the Northern Adriatic Sea at other locations. For example, this genus increased from 10% to 40% in the twentieth century at another site located at 32 m depth in the distal portions of the Po prodelta (Barmawidjaja *et al.* 1995; Van der Zwaan 2000). Similarly, data from cores show that proportional abundances of *V. gibba* increased during the twentieth century at the Po prodelta and in the Gulf of Trieste (Tomašových *et al.* 2018), whereas proportional abundances of *T. tricarinata* declined at the same time (Tomašových *et al.* 2018). The cause of the opposite trend in abundance of *T. tricarinata* in our core can be related to its abundance increase prior to frequent oxygen depletion in the late twentieth century (with the stratigraphic resolution in our core not allowing to distinguish the late twentieth century decline) or to overall less negative side-effects of eutrophication on *T. tricarinata* at the sampling station. Surprisingly, although *Cytheridea neapolitana* tends to inhabit organic-rich sediments and exhibits tolerance to hypoxia (Barbieri *et al.* 2019; Salvi *et al.* 2020), this species declines in proportional abundance at the transition between the shell lag and prodelta silts.

Low sedimentation rates and onshore transport

The up-core decrease in micro- and macrofaunal densities in the prodelta silts, in contrast to the underlying shell lag, can be explained by two phases of increasing sedimentation rate on the basis of stratigraphic profiles in median shell ages: net sedimentation rates increase from *c.* 0.05 mm a^{-1} in the shell lag to 0.15 mm a^{-1} at the base of the prodelta silts and to 0.5 mm a^{-1} at the top of the prodelta silts. The excess ^{210}Pb activity rapidly declines down-core within the upper 10 cm, with the slope indicating sedimentation rate of 0.6 mm a^{-1}. Although some values in the excess ^{210}Pb activity exceeding 10 Bq kg^{-1} at increments below 10 cm indicate a non-local mixing of fine-grained sediment (Fig. 5c), the apparent net sedimentation rates in the prodelta silts based on excess ^{210}Pb activity and on median age ^{14}C data in the uppermost increments are thus congruent. The differences in the shape of age distributions between the 0–2.5 cm and 5–7.5 cm increments show that the present-day surface mixed layer is rather patchy and

is not thicker than 5 cm (Fig. 5a). Median age and time-averaging rapidly increase at 5–7.5 cm increment (with the subset of *V. gibba* shells being coeval with the growth of the rhodolith over several centuries), but the underlying shell lag is age-homogenized at 10–32.5 cm in terms of median ages of *V. gibba* (2880 years at 10–12.5 cm, 4480 years at 17.5–20 cm, and 3570 years at 27.5–32.5 cm, Fig. 5b). Age homogenization of *V. gibba* median ages at 10–30 cm thus indicates that the surface well-mixed layer (a layer characterized by vertical age-homogeneity, i.e. median ages do not monotonically increase down-core) was thicker in the past than during the deposition of the uppermost 10 cm over the last several centuries. With the exception of abundance peaks of a few mollusc and foraminifer species in the uppermost 5 cm of the shell lag, the down-core constancy in proportional abundances of molluscs and foraminifers also indicates that the interval between 45 and 10 cm was homogenized by mixing.

The prodelta silts in the top 10 cm of the core are age-equivalent to less condensed muddy wedge sediments closer to the shore. Po prodelta sediments deposited during the Holocene highstand phase can attain 3–8 m thickness in proximal positions (Amorosi *et al.* 2017), with >100 cm deposited during the twentieth century at water depths around 20 m (Tomašových *et al.* 2018; Riminucci *et al.* 2022). In contrast, the thickness of sediments that overlie the maximum flooding surface at locations eastward of the Po Delta is invariably <20 cm (Picone *et al.* 2008), similarly as at our location. Therefore, on one hand, in spite of the overall progradation, the depositional setting at the core location has been affected by sediment winnowing and transport by currents (and storms), and thus by overall sediment bypassing and starvation due to its distance from the Po della Pila mouth (*c.* 30 km, Fig. 11). On the other hand, the uppermost unit still documents an increase in net sedimentation rate in comparison to the underlying shell lag. This stratigraphic shift in sedimentation rate probably reflects the increase in terrigenous supply due to the onset of more rapid Po delta progradation *c.* 2000 years ago (Amorosi *et al.* 2019) and the subsequent shift of the Po River northwards to its present-day position *c.* 800 years ago (Correggiari *et al.* 2005), which brought the main delta outlets closer to the core site (Fig. 11). A decline in the strength of the thermohaline circulation in the twentieth century (Vilibić *et al.* 2013) could have enhanced the persistence of fine sediments, and thus contributed to higher net sedimentation rates. Although the uppermost 10 cm formed by silts can represent transient or ephemeral deposits at longer geological time scales, this unit is still important in archiving changes in the ecosystem composition that took place over the past centuries.

The age offsets between the intertidal species *L. mediterraneum* and the subtidal species *V. gibba* co-occurring in the upper 60 cm of the core document environmental condensation of benthic assemblages (e.g. Fürsich 1978; Kidwell 1998, 2013). While *V. gibba* shells range in age from several thousand to less than 50 years, *L. mediterraneum* shells are all almost 10 000 years old (Fig. 5a). Although specimens of *L. mediterraneum* occur in the upper part of the core within the *V. gibba*-dominated shell bed, their age range is remarkably narrow relative to the duration of marine deposition at this location. The two species are thus characterized by vastly different scales of time-averaging (IQR of *L. mediterraneum* = 310 years, IQR of *V. gibba* = 3750 years). At 9000–10 000 years ago, when the sea level was around 45 m lower than today, shallow-water shoreface habitats preferred by *L. mediterraneum* were located along the shoreline about 60 km to the SSE relative to the present-day position of the sampling station. *L. mediterraneum* shells were thus extensively transported landwards to the NNW by storms or by tidal currents during the late transgressive phase, to the location of the coring site. In a similar example, Flessa (1998) described the long-distant transport of shells of an intertidal species in landward and seaward directions during the Holocene transgression of the southern North Sea. *L. mediterraneum* in other studies of Holocene transgressive strata in the Northern Adriatic Sea occurs in highly condensed assemblages that underwent sediment reworking and starvation, even in the absence of transport (Scarponi *et al.* 2013, 2017). However, the rarity and poor preservation of the *L. mediterraneum* in our core is inconsistent with very high abundances typically reached by this species in intertidal habitats. Therefore, their low abundance points to lateral transport of a few shells rather than to *in situ* reworking from previous lagoonal or shore-face deposits eroded during the transgression. *L. mediterraneum* thus inhabited habitats during the transgressive phase that were located seaward relative to the sampling site. Ages of plant remains from the lower part of the core demonstrate that the sampling site was at that time still a part of a floodplain.

Decline from millennial to centennial time-averaging resulting from shifts in sedimentation and mixing

Multi-millennial time-averaging and age homogeneity that characterize the shell lag of the transgressive sand sheet were produced by (1) very low net sedimentation rate (owing to winnowing and sediment bypassing induced by longshore currents and storms) and (2) deep bioturbation that age-homogenized the shell lag. These processes led to condensation and co-occurrence of mainly autochthonous–parautochthonous but non-contemporaneous skeletal remains. *V. gibba* shells are mostly well preserved, and probably correspond to autochthonous or parautochthonous assemblages inhabiting the seafloor during sea-level stabilization at shallow-subtidal water depths during the deposition of the shell lag and the overlying prodelta silts. Time-averaging declines markedly across this transition, from millennial scale at 5–32.5 cm to centennial scale at 0–2.5 cm. Although the main decline in time-averaging is located in the lower part of prodelta silts (5–7.5 cm), the age distribution of *V. gibba* is bimodal in this increment. It consists of two age modes with five shells younger than 400 years and five shells older than 2400 years (Fig. 5a, b). Therefore, this shift in the scale of time-averaging was probably pushed upward by recent exhumation of old shells from the lag into the overlying sediment increments by burrowers. The rhodolith that is located at the same sediment depth as the assemblage of *V. gibba* with the bimodal age distribution is coeval with its younger mode. The rhodolith grew *in situ* under very slow sedimentation and occasional overturning by currents for minimum *c.* 300 years at the same time as the shells of *V. gibba* belonging to the younger mode entered into a death assemblage (now at 5–7.5 cm depth). The up-core decline in time-averaging is caused partly by the increase in sedimentation rate (i.e. from *c.* 0.05 mm a^{-1} in the shell lag to *c.* 0.5 mm a^{-1} in the upper 5 cm, Fig. 5d). However, the present-day mixing depth located below the sediment–water interface as shown by shell-age profiles is unusually low, not exceeding 5 cm. This limited thickness contrasts with the 10–20-cm-thick mixed layers (similarly detected on the basis of age-homogeneity of shells) observed at sites with fast and slow sedimentation, e.g. at the Po prodelta (Tomašových *et al.* 2018), in the Gulf of Venice (Gallmetzer *et al.* 2019) or in the NE Adriatic Sea (Tomašových *et al.* 2021). Age-homogeneity of *V. gibba* between 10 and 32.5 cm and the decrease in median age in the uppermost 7.5 cm indicate a temporal decline in intensity of vertical sediment mixing by bioturbation in the twentieth century, further contributing to the limited time-averaging in the uppermost 5 cm. These two factors ultimately allow the preservation of eutrophication proxies in the uppermost portions of the stratigraphic record.

The expression of eutrophication in geochemical and palaeoecological proxies

Increasing major (Al) and trace elements (Cr, Hg, Ni, Pb, Zn), coinciding with a higher content of finer particles, might indicate a change in sediment delivery or a change in source area. Higher values of Ni and

Cr in the upper part of the core can be partly driven by the erosion of ophiolite complexes outcropping in the Western Alps and northwestern Apennines (Bianchini *et al.* 2013; Greggio *et al.* 2017). In surface sediments of Po Delta lagoons, the concentration of Ni exceeds the ERM and despite resulting from natural geological processes, these concentrations can have an ecotoxicological effect (Zonta *et al.* 2019). A significant anthropogenic source of Cr has been identified in the Brenta River (Juracic *et al.* 1986; Nimis *et al.* 2002), due to tanneries and galvanic industries located in its drainage basin. The noticeable increase of Hg concentration in facies 4 (prodelta silts) corresponds to an enrichment that is independent of the grain size effect (i.e. the increase in Hg is unrelated to changes in grain size) observed elsewhere in surface sediments of the Northern Adriatic Sea (Fabbri *et al.* 2001). Consequently, Hg concentration in prodelta silts can be linked to anthropogenic factors. Multiple sources of the Hg enrichment exist in the Northern Adriatic Sea, including cinnabar mining in the Idrija district (western Slovenia), from where Hg is transported by the Isonzo River into the Gulf of Trieste (Covelli *et al.* 2001; Acquavita *et al.* 2012) or waste minerals from industrial processing of zinc in the Gulf of Venice (Donazzolo *et al.* 1981). Main sediment source, and consequently source of heavy metals, at our sampling site is the Po River (Fabbri *et al.* 2001). The observed Hg and Ni concentrations lie below ERM but exceed the ERL and thus might cause ecotoxicological effects.

Elevated concentrations of Pb and Zn in the studied core are consistent with significant enrichment of these two elements found at other locations of the Northern Adriatic Sea (Greggio *et al.* 2017; Natali and Bianchini 2018). Boldrin *et al.* (1992) identified the Adige River as a potential source of Pb for the Adriatic Sea as a consequence of the absorption of this metal on the detrital particles in the drainage basin of the river. Zinc enrichment can reflect an increase in the frequency of boating activities due to its use as biocide agents in antifouling paints (Campos 2003). Zinc is common to all industrial and urban areas, being one of the most used metals in the world (Ademoyero and Gan 1994). Lead enrichment is typically caused by elevated general atmospheric emissions caused by the combustion of fossil fuels used until the beginning of the twenty-first century (Migani *et al.* 2015). Although the strong up-core increase in total nitrogen or total organic carbon in the surface mixed layer is expected owing to diagenesis of organic matter even in the absence of eutrophication, these trends are associated with stratigraphic increase in abundance of taxa preferring organic-rich sediments. In our core, proportional abundances of an organic-loving benthic foraminifer (*Nonionella* sp.) and molluscs

(*V. gibba*, *T. tricarinata*) increase in the uppermost 10 cm. *V. gibba* exhibits an increase in shell size in the same stratigraphic interval. Although centennial-scale time-averaging in the uppermost increments does not allow us to disentangle the specific contributions of eutrophication and pollution at higher, decadal or yearly resolution, the intensification of anthropogenic impacts during the twentieth century is still expressed in the stratigraphic record as distinct trends in abundance and size structure of species responding to eutrophication and changes in concentrations of heavy metals.

Conclusions

The 300 cm-long gravity core preserves the depositional record of the Holocene transgression in the Northern Adriatic Sea, expressed by, from bottom to top: (1) alluvial and transitional sediments assigned to the TST; (2) a shell-rich lag capped by the maximum flooding surface; and (3) a thin veneer of prodelta silts of the HST that preserves the signatures of human impacts such as eutrophication and pollution. Bulk geochemical analyses document a significant increase in the concentrations of major (Al) and trace elements (Cr, Hg, Ni, Pb, Zn), and a strong up-core increase in organic enrichment in the uppermost 10 cm of the core. The distributions of postmortem ages of *V. gibba* shells, as well as the growth and encrustation of the rhodolite, and the excess ^{210}Pb activity reveal a strong shift in sedimentation rate in the younger sedimentation history. Starting from *c.* 0.05 mm a^{-1} during the deposition of the shell lag, the sedimentation rate increased to 0.5 mm a^{-1} during the deposition of prodelta silts (Fig. 5). Shell ages of the bivalve *L. mediterraneum* indicate episodes of landward transport (up to 60 km landwards) and long-term reworking (up to *c.* 10 000 years) during the Holocene transgression. Median ages of *V. gibba* document age-homogenization and millennial time-averaging of molluscs within the shell lag over the past centuries (but prior to the twentieth century). Surprisingly, the overlying 10 cm-thick prodelta silts are not age-homogenized, reflecting a limited thickness of the present-day surface mixed layer owing to the recent decrease in the depth of bioturbation. Owing to the limited present-day mixing and temporarily higher sedimentation, the uppermost core increments thus still capture a decline in grain size and an increase in the proportional abundance and size of species benefiting from eutrophication.

References

Acquavita, A., Covelli, S. *et al.* 2012. Mercury in the sediments of the Marano and Grado Lagoon (northern Adriatic Sea): sources, distribution and speciation. *Estuarine, Coastal and Shelf Science*, **113**, 20–31, https://doi.org/10.1016/j.ecss.2012.02.012

Ademoyero, A.A. and Gan, K.N. 1994. Toxicological profile for zinc. *US Department of Health and Human Services*, **229**.

Albano, P.G., Gallmetzer, I., Haselmair, A., Tomašových, A., Stachowitsch, M. and Zuschin, M. 2018. Historical ecology of a biological invasion: the interplay of eutrophication and pollution determines time lags in establishment and detection. *Biological Invasions*, **20**, 1417–1430, https://doi.org/10.1007/s10530-017-1634-7

Allen, A.P., Kosnik, M.A. and Kaufman, D.S. 2013. Characterizing the dynamics of amino acid racemization using time-dependent reaction kinetics: a Bayesian approach to fitting age-calibration models. *Quaternary Geochronology*, **18**, 63–77, https://doi.org/10.1016/j.quageo.2013.06.003

Allmon, W.D. 2011. Natural history of turritelline gastropods (Cerithiodea: Turritellidae): A status report. *Malacologia*, **54**, 159–202, https://doi.org/10.4002/040.054.0107

Alvisi, F. 2009. A simplified approach to evaluate sedimentary organic matter fluxes and accumulation on the NW Adriatic Shelf (Italy). *Chemistry and Ecology*, **25**, 119–134, https://doi.org/10.1080/0275754090276 2935

Amorosi, A., Centineo, M.C., Colalongo, M.L., Pasini, G., Sarti, G. and Vaiani, S.C. 2003. Facies architecture and Latest Pleistocene-Holocene depositional history of the Po Delta (Comacchio Area), Italy. *Journal of Geology*, **111**, 39–56, https://doi.org/10.1086/344577

Amorosi, A., Pavesi, M., Ricci Lucchi, M., Sarti, G. and Piccin, A. 2008. Climatic signature of cyclic fluvial architecture from the Quaternary of the central Po Plain, Italy. *Sedimentary Geology*, **209**, 58–68, https://doi.org/10.1016/j.sedgeo.2008.06.010

Amorosi, A., Bruno, L. *et al.* 2017. Global sea-level control on local parasequence architecture from the Holocene record of the Po Plain, Italy. *Marine and Petroleum Geology*, **87**, 99–111, https://doi.org/10.1016/j.marpetgeo.2017.01.020

Amorosi, A., Barbieri, G. *et al.* 2019. Three-fold nature of coastal progradation during the Holocene eustatic highstand, Po Plain, Italy – close correspondence of stratal character with distribution patterns. *Sedimentology*, **66**, 3029–3052, https://doi.org/10.1111/sed.12621

Amorosi, A., Bruno, L., Campo, B., Di Martino, A. and Sammartino, I. 2021. Patterns of geochemical variability across weakly developed paleosol profiles and their role as regional stratigraphic markers (Upper Pleistocene, Po Plain). *Palaeogeography, Palaeoclimatology, Palaeoecology*, **574**, 110413, https://doi.org/10.1016/j.palaeo.2021.110413

Bada, J.L. and McDonald, G.D. 1995. Amino acid racemization on mars: implications for the preservation of biomolecules from an extinct martian biota. *Icarus*, **114**, 139–143, https://doi.org/10.1006/icar.1995.1049

Barbieri, G., Rossi, V., Vaiani, S.C. and Horton, B.P. 2019. Benthic ostracoda and foraminifera from the North Adriatic Sea (Italy, Mediterranean Sea): a proxy for the depositional characterisation of river-influenced shelves. *Marine Micropaleontology*, **153**, 101772, https://doi.org/10.1016/j.marmicro.2019.101772

Barmawidjaja, D.M., van der Zwaan, G.J., Jorissen, F.J. and Puskaric, S. 1995. 150 years of eutrophication in

the northern Adriatic Sea: evidence from a benthic fora-miniferal record. *Marine Geology*, **122**, 367–384, https://doi.org/10.1016/0025-3227(94)00121-Z

Basso, D. 1998. Deep rhodolith distribution in the Pontian Islands, Italy: a model for the paleoecology of a temperate sea. *Palaeogeography, Palaeoclimatology, Palaeoecology*, **137**, 173–187, https://doi.org/10.1016/S0031-0182(97)00099-0

Bianchini, G., di Giuseppe, D., Natali, C. and Beccaluva, L. 2013. Ophiolite inheritance in the Po Plain sediments: insights on heavy metals distribution and risk assessment. *Ofioliti*, **38**, 1–14, https://doi.org/10.4454/ofio liti.v38i1.412

Birks, H.J.B. 2012. Analysis of stratigraphical data. *In*: Birks, H.J.B., Lotter, A.F., Juggins, S. and Smol, J.P. (eds) *Tracking Environmental Change Using Lake Sediments: Data Handling and Numerical Techniques*. Springer, Dordrecht, 355–378, https://doi.org/10.1007/978-94-007-2745-8_11

Boldrin, A., Juracić, M., Menegazzo Vitturi, L., Rabitti, S. and Rampazzo, G. 1992. Sedimentation of riverborne material in a shallow shelf sea: Adige River, Adriatic Sea. *Marine Geology*, **103**, 473–485, https://doi.org/10.1016/0025-3227(92)90033-E

Boldrin, A., Carniel, S. *et al.* 2009. Effects of bora wind on physical and biogeochemical properties of stratified waters in the northern Adriatic. *Journal of Geophysical Research*, **114**, 1–19, https://doi.org/10.1029/2008jc004837

Bozzeda, F. 2010. Impatto degli interventi antropici di difesa costiera sulla struttura e distribuzione della popolazione di *Lentidium mediterraneum* (Mollusca bivalvia). Diploma thesis, University of Bologna.

Bruno, L., Bohacs, K.M. *et al.* 2017. Early Holocene transgressive palaeogeography in the Po coastal plain (northern Italy). *Sedimentology*, **64**, 1792–1816, https://doi.org/10.1111/sed.12374

Burton, G.A., Kumagai, M., Hashitani, H. and Tanimoto, R. 2004. Sediment quality criteria in use around the world. *Japanese Journal of Limnology*, **65**, 117–134, https://doi.org/10.3739/rikusui.65.117

Bush, S.L., Santos, G.M., Xu, X., Southon, J.R., Thiagarajan, N., Hines, S.K. and Adkins, J.F. 2013. Simple, rapid, and cost effective: a screening method for ^{14}C analysis of small carbonate samples. *Radiocarbon*, **55**, 631–640, https://doi.org/10.1017/s0033822200057787

Campo, B., Amorosi, A. and Vaiani, S.C. 2017. Sequence stratigraphy and late Quaternary paleoenvironmental evolution of the Northern Adriatic coastal plain (Italy). *Palaeogeography, Palaeoclimatology, Palaeoecology*, **466**, 265–278, https://doi.org/10.1016/j.palaeo.2016.11.016

Campos, V. 2003. Trace elements in pesticides. *Communications in Soil Science and Plant Analysis*, **34**, 1261–1268, https://doi.org/10.1081/CSS-120020442

Cattaneo, A. and Steel, R.J. 2003. Transgressive deposits: a review of their variability. *Earth-Science Reviews*, **62**, 187–228, https://doi.org/10.1016/S0012-8252(02)00134-4

Catuneanu, O., Abreu, V. *et al.* 2009. Towards the standardization of sequence stratigraphy. *Earth-Science Reviews*, **92**, 1–33, https://doi.org/10.1016/j.earscirev.2008.10.003

Chiantore, M., Bedulli, D., Cattaneo-Vietti, R., Schiaparelli, S. and Albertelli, G. 2001. Long-term changes in the Mollusc-Echinoderm assemblages in the north and coastal middle Adriatic Sea. *Atti della Associazione Italiana di Oceanologia e Limnologia*, **14**, 63–75.

Colantoni, P., Gallignani, P. and Lenaz, R. 1979. Late Pleistocene and Holocene evolution of the North Adriatic continental shelf (Italy). *Marine Geology*, **33**, M41–M50, https://doi.org/10.1016/0025-3227(79)90130-0

Correggiari, A., Field, M.E. and Trincardi, F. 1996*a*. Late Quaternary transgressive large dunes on the sediment-starved Adriatic shelf. *Geological Society, London, Special Publications*, **117**, 155–169, https://doi.org/10.1144/GSL.SP.1996.117.01.09

Correggiari, A., Roveri, M. and Trincardi, F. 1996*b*. Late Pleistocene and Holocene evolution of the Northern Adriatic Sea. *Italian Journal of Quaternary Sciences*, **9**, 697–704.

Correggiari, A., Cattaneo, A. and Trincardi, F. 2005. Depositional patterns in the late holocene po delta system. *SEPM Special Publications*, **83**, 365–392, https://doi.org/10.2110/pec.05.83.0365

Covelli, S. and Fontolan, G. 1997. Application of a normalization procedure in determining regional geochemical baselines: Gulf of Trieste, Italy. *Environmental Geology*, **30**, 34–45, https://doi.org/10.1007/s002540050130

Covelli, S., Faganeli, J., Horvat, M. and Brambati, A. 2001. Mercury contamination of coastal sediments as the result of long-term cinnabar mining activity (Gulf of Trieste, northern Adriatic sea). *Applied Geochemistry*, **16**, 541–558, https://doi.org/10.1016/S0883-2927(00)00042-1

Covelli, S., Fontolan, G., Faganeli, J. and Ogrinc, N. 2006. Anthropogenic markers in the Holocene stratigraphic sequence of the Gulf of Trieste (northern Adriatic Sea). *Marine Geology*, **230**, 29–51, https://doi.org/10.1016/j.margeo.2006.03.013

Cozzi, S., Cabrini, M., Kralj, M., De Vittor, C., Celio, M. and Giani, M. 2020. Climatic and anthropogenic impacts on environmental conditions and phytoplankton community in the Gulf of Trieste (Northern Adriatic Sea). *Water*, **12**, 2652, https://doi.org/10.3390/w12092652

Crema, E.R. and Bevan, A. 2021. Inference from large sets of radiocarbon dates: software and methods. *Radiocarbon*, **63**, 23–39, https://doi.org/10.1017/RDC.2020.95

Crema, R., Castelli, A. and Prevedelli, D. 1991. Long term eutrophication effects on macrofaunal communities in Northern Adriatic Sea. *Marine Pollution Bulletin*, **22**, 503–508, https://doi.org/10.1016/0025-326X(91)90405-H

Croudace, I.W. and Rothwell, R.G. 2015. Micro-XRF studies of sediment cores. *Applications of a Non-Destructive Tool for the Environmental Sciences*, Springer, https://doi.org/10.1007/978-94-017-9849-5

Degobbis, D. 1989. Increased eutrophication of the northern Adriatic sea. Second act. *Marine Pollution Bulletin*, **20**, 452–457, https://doi.org/10.1016/0025-326X(89)90066-0

Djakovac, T., Degobbis, D., Supić, N. and Precali, R. 2012. Marked reduction of eutrophication pressure in the northeastern Adriatic in the period 2000–2009.

Human impacts in condensed shelf deposits

Estuarine, Coastal and Shelf Science, **115**, 25–32, https://doi.org/10.1016/j.ecss.2012.03.029

Dolven, J.K., Alve, E., Rygg, B. and Magnusson, J. 2013. Defining past ecological status and in situ reference conditions using benthic foraminifera: a case study from the Oslofjord, Norway. *Ecological Indicators*, **29**, 219–233, https://doi.org/10.1016/j.ecolind.2012.12.031

Donazzolo, R., Merlin, O.H., Vitturi, L.M., Orio, A.A., Pavoni, B., Perin, G. and Rabitti, S. 1981. Heavy metal contamination in surface sediments from the Gulf of Venice, Italy. *Marine Pollution Bulletin*, **12**, 417–425, https://doi.org/10.1016/0025-326X(81)90160-0

Fabbri, D., Gabbianelli, G., Locatelli, C., Lubrano, D., Trombini, C. and Vassura, I. 2001. Distribution of mercury and other heavy metals in core sediments of the northern Adriatic Sea. *Water, Air, and Soil Pollution*, **129**, 143–153, https://doi.org/10.1023/A:1010304727271

Faganeli, J., Pezdič, J., Ogorelec, B., Herndl, G.J. and Dolenec, T. 1991. The role of sedimentary biogeochemistry in the formation of hypoxia in shallow coastal waters (Gulf of Trieste, northern Adriatic). *Geological Society, London, Special Publications*, **58**, 107–117, https://doi.org/10.1144/GSL.SP.1991.058.01.08

Fairchild, I., Zalasiewicz, J. *et al*. 2019. Anthropocene chemostratigraphy. *In*: Zalasiewicz, J., Waters, C.N., Williams, M. and Summerhayes, C.P. (eds) *The Anthropocene as a Geological Time Unit: A Guide to the Scientific Evidence and Current Debate*. Cambridge University Press, 156–159.

Flessa, K.W. 1998. Well-traveled cockles: shell transport during the Holocene transgression of the southern North Sea. *Geology*, **26**, 187–190, https://doi.org/10.1130/0091-7613(1998)026<0187:WTCSTD>2.3.CO;2

Flessa, K.W., Cutler, A.H. and Meldahl, K.H. 1993. Time and taphonomy: quantitative estimates of time-averaging and stratigraphic disorder in a shallow marine habitat. *Paleobiology*, **19**, 266–286, https://doi.org/10.1017/S0094837300015918

Föllmi, K.B. 2016. Sedimentary condensation. *Earth-Science Reviews*, **152**, 143–180, https://doi.org/10.1016/j.earscirev.2015.11.016

Frascari, F., Frignani, M., Guerzoni, S. and Ravaioli, M. 1988. Sediments and Pollution in the Northern Adriatic Sea. *Annals of the New York Academy of Sciences*, **534**, 1000–1020, https://doi.org/10.1111/j.1749-6632.1988.tb30191.x

Frignani, M. and Langone, L. 1991. Accumulation rates and 137Cs distribution in sediments off the Po River delta and the Emilia-Romagna coast (northwestern Adriatic Sea, Italy). *Continental Shelf Research*, **11**, 525–542, https://doi.org/10.1016/0278-4343(91)90009-U

Frignani, M., Langone, L., Ravaioli, M., Sorgente, D., Alvisi, F. and Albertazzi, S. 2005. Fine-sediment mass balance in the western Adriatic continental shelf over a century time scale. *Marine Geology*, **222–223**, 113–133, https://doi.org/10.1016/j.margeo.2005.06.016

Fürsich, F.T. 1978. The influence of faunal condensation and mixing on the preservation of fossil benthic

communities. *Lethaia*, **11**, 243–250, https://doi.org/10.1111/j.1502-3931.1978.tb01231.x

Fuksi, T., Tomašových, A., Gallmetzer, I., Haselmair, A. and Zuschin, M. 2018. 20th century increase in body size of a hypoxia-tolerant bivalve documented by sediment cores from the northern Adriatic Sea (Gulf of Trieste). *Marine Pollution Bulletin*, **135**, 361–375, https://doi.org/10.1016/j.marpolbul.2018.07.004

Gallmetzer, I., Haselmair, A., Tomašových, A., Stachowitsch, M. and Zuschin, M. 2017. Responses of molluscan communities to centuries of human impact in the northern Adriatic Sea. *PLoS One*, **12**, e0180820, https://doi.org/10.1371/journal.pone.0180820

Gallmetzer, I., Haselmair, A. *et al*. 2019. Tracing origin and collapse of Holocene benthic baseline communities in the northern Adriatic Sea. *PALAIOS*, **34**, 121–145, https://doi.org/10.2110/palo.2018.068

Giani, M., Djakovac, T., Degobbis, D., Cozzi, S., Solidoro, C. and Umani, S.F. 2012. Recent changes in the marine ecosystems of the northern Adriatic Sea. *Estuarine, Coastal and Shelf Science*, **115**, 1–13, https://doi.org/10.1016/j.ecss.2012.08.023

Gibbard, P., Walker, M. *et al*. 2022. The Anthropocene as an Event, not an Epoch. *Journal of Quaternary Science*, **37**, 395–399, https://doi.org/10.1002/jqs.3416

Greggio, N., Giambastiani, B.M.S., Campo, B., Dinelli, E. and Amorosi, A. 2017. Sediment composition, provenance, and Holocene paleoenvironmental evolution of the Southern Po River coastal plain (Italy). *Geological Journal*, **53**, 914–928, https://doi.org/10.1002/gj.2934

Grilli, F., Accoroni, S. *et al*. 2020. Seasonal and interannual trends of oceanographic parameters over 40 years in the northern Adriatic Sea in relation to nutrient loadings using the EMODnet chemistry data portal. *Water*, **12**, 2280, https://doi.org/10.3390/w12082280

Haselmair, A., Gallmetzer, I., Tomašových, A., Wieser, A., Übelhör, A. and Zuschin, M. 2021. Basin-wide infaunalisation of benthic soft-bottom communities driven by anthropogenic habitat degradation in the northern Adriatic Sea. *Marine Ecology Progress Series*, **671**, 45–65, https://doi.org/10.3354/meps13759

Heaton, T.J., Köhler, P. *et al*. 2020. Marine20 – The Marine Radiocarbon Age Calibration Curve (0–55 000 cal BP). *Radiocarbon*, **62**, 779–820, https://doi.org/10.1017/RDC.2020.68

Hrs-Brenko, M. 2006. The basket shell, *Corbula gibba* Olivi, 1792 (Bivalve Mollusks) as a species resistant to environmental disturbances: a review. *Acta Adriatica: International journal of Marine Sciences*, **47**, 49–64, http://jadran.izor.hr/acta/pdf/47_1_pdf/47_1_6.pdf

Ingram, W.C., Meyers, S.R., Brunner, C.A. and Martens, C.S. 2010. Late Pleistocene-Holocene sedimentation surrounding an active seafloor gas-hydrate and cold-seep field on the Northern Gulf of Mexico Slope. *Marine Geology*, **278**, 43–53, https://doi.org/10.1016/j.margeo.2010.09.002

Juggins, S. 2015. *Rioja: analysis of Quaternary Science data. R package version 1.0-5*, https://cran.r-project.org/package=rioja

Juracic, M., Vitturi, L.M., Rabitti, S. and Rampazzo, G. 1986. Suspended matter properties and its role in pollutant transfer from the river to the sea. Case study: Adige river-Adriatic Sea. *Science of the Total Environment*,

55, 243–249, https://doi.org/10.1016/0048-9697(86)90183-X

Justić, D. 1988. Trend in the transparency of the northern Adriatic Sea 1911-1982. *Marine Pollution Bulletin*, **19**, 32–35, https://doi.org/10.1016/0025-326X(88)90751-5

Justić, D. 1991. Hypoxic conditions in the northern Adriatic Sea: historical development and ecological significance. *Geological Society, London, Special Publications*, **58**, 95–105, https://doi.org/10.1144/GSL.SP.1991.058.01.0

Kidwell, S.M. 1986. Taphonomic feedback in Miocene assemblages: testing the role of dead hardparts in benthic communities. *PALAIOS*, **1**, 239–255, https://doi.org/10.2307/3514688

Kidwell, S.M. 1998. Time-averaging in the marine fossil record: overview of strategies and uncertainties. *Oceanographic Literature Review*, **9**, 1546–1547.

Kidwell, S.M. 2013. Time-averaging and fidelity of modern death assemblages: building a taphonomic foundation for conservation palaeobiology. *Palaeontology*, **56**, 487–522, https://doi.org/10.1111/pala.12042

Kosnik, M.A., Hua, Q., Jacobsen, G.E., Kaufman, D.S. and Wüst, R.A. 2007. Sediment mixing and stratigraphic disorder revealed by the age-structure of *Tellina* shells in Great Barrier Reef sediment. *Geology*, **35**, 811–814, https://doi.org/10.1130/G23722A.1

Kowalewski, M. 1996. Time-averaging, overcompleteness, and the geological record. *The Journal of Geology*, **104**, 317–326, https://doi.org/10.1086/629827

Kowalewski, M., Wittmer, J.M., Dexter, T.A., Amorosi, A. and Scarponi, D. 2015. Differential responses of marine communities to natural and anthropogenic changes. *Proceedings of the Royal Society B: Biological Sciences*, **282**, https://doi.org/10.1098/rspb.2014.2990

Kralj, M., Lipizer, M. *et al.* 2019. Hypoxia and dissolved oxygen trends in the northeastern Adriatic Sea (Gulf of Trieste). *Deep Sea Research Part II: Topical Studies in Oceanography*, **164**, 74–88, https://doi.org/10.1016/j.dsr2.2019.06.002

Kuzyk, Z.Z.A., Macdonald, R.W. and Johannessen, S.C. 2015. Calculating rates and dates and interpreting contaminant profiles in biomixed sediments. *In*: Blais, J., Rosen, M. and Smol, J. (eds) *Environmental Contaminants*. Springer, Dordrecht, 61–87, https://doi.org/10.1007/978-94-017-9541-8_4

Lamb, A.L., Wilson, G.P. and Leng, M.J. 2006. A review of coastal palaeoclimate and relative sea-level reconstructions using d^{13}C and C/N ratios in organic material. *Earth-Science Reviews*, **75**, 29–57, https://doi.org/10.1016/j.earscirev.2005.10.003

Lambeck, K., Rouby, H., Purcell, A., Sun, Y. and Sambridge, M. 2014. Sea level and global ice volumes from the Last Glacial Maximum to the Holocene. *Proceedings of the National Academy of Sciences*, **111**, 15296–15303, https://doi.org/10.1073/pnas.1411762111

Langone, L., Asioli, A., Correggiari, A. and Trincardi, F. 1996. Age-depth modelling through the late Quaternary deposits of the central Adriatic basin. *Memorie-Istituto Italiano Di Idrobiologia*, **55**, 177–196.

Lewis, S.L. and Maslin, M.A. 2015. Defining the Anthropocene. *Nature*, **519**, 171–180, https://doi.org/10.1038/nature14258

Long, E.R., Macdonald, D.D., Smith, S.L. and Calder, F.D. 1995. Incidence of adverse biological effects within ranges of chemical concentrations in marine and estuarine sediments. *Environmental Management*, **19**, 81–97, https://doi.org/10.1007/BF02472006

Loring, D.H. 1991. Normalization of heavy-metal data from estuarine and coastal sediments. *ICES Journal of Marine Science*, **48**, 101–115, https://doi.org/10.1093/icesjms/48.1.101

Malvern Instruments Ltd 2007. *User's Manual: Mastersizer 2000*. Malvern Instruments Ltd.

Marchetti, R., Provini, A. and Crosa, G. 1989. Nutrient load carried by the River Po into the Adriatic Sea, 1968–1987. *Marine Pollution Bulletin*, **20**, 168–172, https://doi.org/10.1016/0025-326X(89)90487-6

Marsh, R., Mills, R.A., Green, D.R.H., Salter, I. and Taylor, S. 2007. Controls on sediment geochemistry in the Crozet region. *Deep-Sea Research Part II: Topical Studies in Oceanography*, **54**, 2260–2274, https://doi.org/10.1016/j.dsr2.2007.06.004

Migani, F., Borghesi, F. and Dinelli, E. 2015. Geochemical characterization of surface sediments from the northern Adriatic wetlands around the Po river delta. Part I: Bulk composition and relation to local background. *Journal of Geochemical Exploration*, **156**, 72–88, https://doi.org/10.1016/j.gexplo.2015.05.003

Moscon, G. 2016. Variability of Late-Quaternary transgressive sedimentation in the Northern Adriatic Sea. Doctoral thesis, University of Padova.

Natali, C. and Bianchini, G. 2018. Natural vs anthropogenic components in sediments from the Po River delta coastal lagoons (NE Italy). *Environmental Science and Pollution Research*, **25**, 2981–2991, https://doi.org/10.1007/s11356-017-0986-y

Nawrot, R., Berensmeier, M., Gallmetzer, I., Haselmair, A., Tomašových, A. and Zuschin, M. 2022. Multiple phyla, one time resolution? Similar time averaging in benthic foraminifera, mollusk, echinoid, crustacean, and otolith fossil assemblages. *Geology*, **50**, 902–906, https://doi.org/10.1130/G49970.1

Nerlović, V., Doğan, A. and Hrs-Brenko, M. 2011. Response to oxygen deficiency (depletion): Bivalve assemblages as an indicator of ecosystem instability in the northern Adriatic Sea. *Biologia*, **66**, 1114–1126, https://doi.org/10.2478/s11756-011-0121-3

Nieuwenhuize, J., Maas, Y.E.M. and Middelburg, J.J. 1994. Rapid analysis of organic carbon and nitrogen in particulate materials. *Marine Chemistry*, **45**, 217–224, https://doi.org/10.1016/0304-4203(94)90005-1

Nimis, P.L., Fumagalli, F., Bizzotto, A., Codogno, M. and Skert, N. 2002. Bryophytes as indicators of trace metal pollution in the River Brenta (NE Italy). *Science of the Total Environment*, **286**, 233–242, https://doi.org/10.1016/S0048-9697(01)00979-2

Novak, A., Šmuc, A., Poglajen, S., Celarc, B. and Vrabec, M. 2020. Sound velocity in a thin shallowly submerged terrestrial-marine Quaternary succession (Northern Adriatic Sea). *Water (Switzerland)*, **12**, https://doi.org/10.3390/w12020560

Ogorelec, B., Mišič, M. and Faganeli, J. 1991. Marine geology of the Gulf of Trieste (northern Adriatic): sedimentological aspects. *Marine Geology*, **99**, 79–92, https://doi.org/10.1016/0025-3227(91)90084-H

Human impacts in condensed shelf deposits

Palinkas, C.M. and Nittrouer, C.A. 2007. Modern sediment accumulation on the Po shelf, Adriatic Sea. *Continental Shelf Research*, **27**, 489–505, https://doi.org/10.1016/j.csr.2006.11.006

Patzkowsky, M.E. and Holland, S.M. 2012. *Stratigraphic Paleobiology*. University of Chicago Press.

Percival, J.B. and Lindsay, P.J. 1997. Measurement of physical properties of sediments. *In*: Mudrock, A., Azcue, J.M. and Mudroch, P. (eds) *Manual of Physico-Chemical Analysis of Aquatic Sediments*. CRC Press, Boca Raton, FL, 7–45, https://doi.org/10.1201/978020 3748176

Picone, S., Alvisi, F., Dinelli, E., Morigi, C., Negri, A., Ravaioli, M. and Vaccaro, C. 2008. New insights on late Quaternary palaeogeographic setting in the Northern Adriatic Sea (Italy). *Journal of Quaternary Science*, **23**, 489–501, https://doi.org/10.1002/jqs.1152

Rabalais, N.N., Turner, R.E., Gupta, B.K., Sen Platon, E. and Parsons, M.L. 2007. Sediments tell the history of eutrophication and hypoxia in the northern Gulf of Mexico. *Ecological Applications*, **17**, 129–143, https://doi.org/10.1890/06-0644.1

RCoreTeam 2021. R: a language and environment for statistical computing. R Foundation for Statistical Computing, Vienna, Austria, https://www.r-project.org/

Reimer, P.J. and Reimer, R.W. 2001. A marine reservoir correction database and on-line interface. *Radiocarbon*, **43**, 461–463, https://doi.org/10.1017/S0033822200 038339

Reimer, P.J., Austin, W.E.N. *et al.* 2020. The IntCal20 Northern Hemisphere Radiocarbon Age Calibration Curve (0–55 cal kBP). *Radiocarbon*, **62**, 725–757, https://doi.org/10.1017/RDC.2020.41

Riminucci, F., Funari, V., Ravaioli, M. and Capotondi, L. 2022. Trace metals accumulation on modern sediments from Po river prodelta, North Adriatic Sea. *Marine Pollution Bulletin*, **175**, 113399, https://doi.org/10.1016/j.marpolbul.2022.113399

Rossi, V. and Vaiani, S.C. 2008. Benthic foraminiferal evidence of sediment supply changes and fluvial drainage reorganization in Holocene deposits of the Po Delta, Italy. *Marine Micropaleontology*, **69**, 106–118, https://doi.org/10.1016/j.marmicro.2008.07.001

Rothwell, R. 2015. Twenty years of XRF core scanning marine sediments: what do geochemical proxies tell us? *In*: Croudacxe, I.W. and Rothwell, R.G. (eds) *Micro-XRF Studies of Sediment Cores. Applications of a non-destructive tool for the environmental sciences*. Springer, 25–102.

Rothwell, R., Hoogakker, B., Thomson, J., Croudace, I. and Frenz, M. 2006. Turbidite emplacement on the southern Balearic Abyssal Plain (western Mediterranean Sea) during Marine Isotope Stages 1–3: an application of ITRAX XRF scanning of sediment cores to lithostratigraphic analysis. *Geological Society, London, Special Publications*, **267**, 79–98, https://doi.org/10.1144/GSL.SP.2006.267.01.06

RstudioTeam 2021. RStudio: Integrated Development Environmet for R, http://www.rstudio.com/

Salvi, G., Acquavita, A., Celio, M., Ciriaco, S., Cirilli, S., Fernetti, M. and Pugliese, N. 2020. Ostracod fauna: eyewitness to fifty years of anthropic impact in the Gulf of Trieste. A potential key to the future evolution

of urban ecosystems. *Sustainability (Switzerland)*, **12**, https://doi.org/10.3390/SU12176954

Sanchez-Cabeza, J.A. and Ruiz-Fernández, A.C. 2012. ^{210}Pb sediment radiochronology: an integrated formulation and classification of dating models. *Geochimica et Cosmochimica Acta*, **82**, 183–200, https://doi.org/10.1016/j.gca.2010.12.024

Sawyer, J.A. and Zuschin, M. 2010. Intensities of drilling predation of molluscan assemblages along a transect through the northern Gulf of Trieste (Adriatic Sea). *Palaeogeography, Palaeoclimatology, Palaeoecology*, **285**, 152–173, https://doi.org/10.1016/j.palaeo.2009.11.007

Scarponi, D., Kaufman, D., Amorosi, A. and Kowalewski, M. 2013. Sequence stratigraphy and the resolution of the fossil record. *Geology*, **41**, 239–242, https://doi.org/10.1130/G33849.1

Scarponi, D., Azzarone, M., Kusnerik, K., Amorosi, A., Bohacs, K.M., Drexler, T.M. and Kowalewski, M. 2017. Systematic vertical and lateral changes in quality and time resolution of the macrofossil record: Insights from Holocene transgressive deposits, Po coastal plain, Italy. *Marine and Petroleum Geology*, **87**, 128–136, https://doi.org/10.1016/j.marpetgeo.2017.03.031

Schlager, W. 1993. Accommodation and supply – a dual control on stratigraphic sequences. *Sedimentary Geology*, **86**, 111–136, https://doi.org/10.1016/0037-0738(93)90136-S

Simboura, N. and Zenetos, A. 2002. Benthic indicators to use in Ecological Quality classification of Mediterranean soft bottom marine ecosystems, including a new Biotic Index. *Mediterranean Marine Science*, **3**, 77–111, https://doi.org/10.12681/mms.249

Spagnoli, F., Dinelli, E., Giordano, P., Marcaccio, M., Zaffagnini, F. and Frascari, F. 2014. Sedimentological, biogeochemical and mineralogical facies of Northern and Central Western Adriatic Sea. *Journal of Marine Systems*, **139**, 183–203, https://doi.org/10.1016/j.jmarsys.2014.05.021

Stachowitsch, M. 1991. Anoxia in the Northern Adriatic Sea: rapid death, slow recovery. *Geological Society, London, Special Publications*, **58**, 119–129, https://doi.org/10.1144/GSL.SP.1991.058.01.09

Storms, J.E.A., Weltje, G.J., Terra, G.J., Cattaneo, A. and Trincardi, F. 2008. Coastal dynamics under conditions of rapid sea-level rise: late Pleistocene to Early Holocene evolution of barrier-lagoon systems on the northern Adriatic shelf (Italy). *Quaternary Science Reviews*, **27**, 1107–1123, https://doi.org/10.1016/j.quascirev.2008.02.009

Sucharovà, J., Suchara, I. *et al.* 2012. Top-/bottom-soil ratios and enrichment factors: what do they really show? *Applied Geochemistry*, **27**, 138–145, https://doi.org/10.1016/j.apgeochem.2011.09.025

Tomašových, A. and Kidwell, S.M. 2010. The effects of temporal resolution on species turnover and on testing metacommunity models. *American Naturalist*, **175**, 587–606, https://doi.org/10.1086/651661

Tomašových, A., Kidwell, S.M., Barber, R.F. and Kaufman, D.S. 2014. Long-term accumulation of carbonate shells reflects a 100-fold drop in loss rate. *Geology*, **42**, 819–822, https://doi.org/10.1130/G35694.1

Tomašových, A., Gallmetzer, I., Haselmair, A., Kaufman, D.S., Vidović, J. and Zuschin, M. 2017. Stratigraphic unmixing reveals repeated hypoxia events over the

past 500 yr in the northern Adriatic Sea. *Geology*, **45**, 363–366, https://doi.org/10.1130/G38676.1

Tomašových, A., Gallmetzer, I. *et al.* 2018. Tracing the effects of eutrophication on molluscan communities in sediment cores: outbreaks of an opportunistic species coincide with reduced bioturbation and high frequency of hypoxia in the Adriatic Sea. *Paleobiology*, **44**, 575–602, https://doi.org/10.1017/pab.2018.22

Tomašových, A., Gallmetzer, I., Haselmair, A., Kaufman, D.S., Mavrič, B. and Zuschin, M. 2019. A decline in molluscan carbonate production driven by the loss of vegetated habitats encoded in the Holocene sedimentary record of the Gulf of Trieste. *Sedimentology*, **66**, 781–807, https://doi.org/10.1111/sed.12516

Tomašových, A., Albano, P.G. *et al.* 2020. Ecological regime shift preserved in the Anthropocene stratigraphic record. *Proceedings of the Royal Society B*, **287**, 20200695, https://doi.org/10.1098/rspb.2020.0695rspb20200695

Tomašových, A., Gallmetzer, I., Haselmair, A. and Zuschin, M. 2021. Inferring time averaging and hiatus durations in the stratigraphic record of high-frequency depositional sequences. *Sedimentology*, **69**, 1083–1118, https://doi.org/10.1111/sed.12936

Trincardi, F., Correggiari, A. and Roveri, M. 1994. Late Quaternary transgressive erosion and deposition in a modern epicontinental shelf: the Adriatic semienclosed basin. *Geo-Marine Letters*, **14**, 41–51, https://doi.org/10.1007/BF01204470

Trincardi, F. and Argagni, A. 2003. *Carta geologica dei mari italiani, scala 1: 250.000, foglio NL 33-10 Ravenna*. Servizio Geologico Nazionale, 2.

Trincardi, F., Argnani, A. and Correggiari, A. 2002. *Carta geologica dei mari italiani, scala 1: 250.000, foglio NL 33-7 Venezia. Servizio Geologico Nazionale*, https://www.isprambiente.gov.it/Media/carg/marine/NL_33_7_VENEZIA_SUP/Foglio.html

Trincardi, F., Argnani, A. and Correggiari, A. 2011. *Note illustrative della Carta Geologica dei Mari Italiani alla scala 1:250.000 – Foglio NL 33-7 Venezia*. ISPRA, Istituto Superiore per la Protezione e la Ricerca Ambientale, Foglio NL, 0–151.

USEPA, United States Environmental Protection Agency 1976. Method 245.1, Mercury. Manual Cold Vapor Technique.

USEPA, United States Environmental Protection Agency 1994. Method 200.7, Determination of Metals and Trace Elements in Water and Wastes by Inductively Coupled Plasma-Atomic Emission Spectrometry.

USEPA, United States Environmental Protection Agency 2007. Method 3051A, Microwave Assisted Acid Digestion of Sediments, Sludges, and Oils- Revision 1.

Van der Zwaan, G.J. 2000. Variation in natural v. anthropogenic eutrophication of shelf areas in front of major rivers. *In*: Martin, R.E. (ed.) *Environmental Micropaleontology*. Springer, 385–404, https://doi.org/10.1007/978-1-4615-4167-7_18

Van der Zwaan, G.J. and Jorissen, F.J. 1991. Biofacial patterns in river-induced shelf anoxia. *Geological Society, London, Special Publications*, **58**, 65–82, https://doi.org/10.1144/GSL.SP.1991.058.01.05

Vatova, A. 1949. La fauna bentonica dell'Alto e Medio Adriatico. *Nova Thalassia*, **3**, 1–110.

Vidovic, J., Nawrot, R. *et al.* 2016. Anthropogenically induced environmental changes in the northeastern Adriatic Sea in the last 500 years (Panzano Bay, Gulf of Trieste). *Biogeosciences (online)*, **13**, 5965–5981, https://doi.org/10.5194/bg-13-5965-2016

Vilibić, I., Šepić, J. and Proust, N. 2013. Weakening thermohaline circulation in the Adriatic Sea. *Climate Research*, **55**, 217–225, https://doi.org/10.3354/cr01128

Weber, K. and Zuschin, M. 2013. Delta-associated molluscan life and death assemblages in the northern Adriatic Sea: Implications for paleoecology, regional diversity and conservation. *Palaeogeography, Palaeoclimatology, Palaeoecology*, **370**, 77–91, https://doi.org/10.1016/j.palaeo.2012.11.021

Wentworth, C.K. 1922. A scale of grade and class terms for clastic sediments. *The Journal of Geology*, **30**, 377–392, https://doi.org/10.1086/622910

Wilkinson, I.P., Poirier, C., Head, M.J., Sayer, C.D. and Tibby, J. 2014. Microbiotic signatures of the Anthropocene in marginal marine and freshwater palaeoenvironments. *Geological Society, London, Special Publications*, **395**, 185–219, https://doi.org/10.1144/SP395.14

Woodward, C.A. and Gadd, P.S. 2019. The potential power and pitfalls of using the X-ray fluorescence molybdenum incoherent: coherent scattering ratio as a proxy for sediment organic content. *Quaternary International*, **514**, 30–43, https://doi.org/10.1016/j.quaint.2018.11.031

Wolfe, A.P., Hobbs, W.O. *et al.* 2013. Stratigraphic expressions of the Holocene–Anthropocene transition revealed in sediments from remote lakes. *Earth-Science Reviews*, **116**, 17–34, https://doi.org/10.1016/j.earscirev.2012.11.001

Zecchin, M., Catuneanu, O. and Caffau, M. 2019. Wave-ravinement surfaces: Classification and key characteristics. *Earth-Science Reviews*, **188**, 210–239, https://doi.org/10.1016/j.earscirev.2018.11.011

Zonta, R., Botter, M., Cassin, D., Bellucci, L.G., Pini, R. and Dominik, J. 2018. Sediment texture and metal contamination in the Venice Lagoon (Italy): a snapshot before the installation of the MOSE system. *Estuarine, Coastal and Shelf Science*, **205**, 131–151, https://doi.org/10.1016/j.ecss.2018.03.007

Zonta, R., Cassin, D., Pini, R. and Dominik, J. 2019. Assessment of heavy metal and as contamination in the surface sediments of Po delta lagoons (Italy). *Estuarine, Coastal and Shelf Science*, **225**, 106235, https://doi.org/10.1016/j.ecss.2019.05.017

Zonta, R., Fontolan, G., Cassin, D. and Dominik, J. 2021. X-ray computed tomography as a tool for screening sediment cores: an application to the lagoons of the Po river delta (Italy). *Journal of Marine Science and Engineering*, **9**, https://doi.org/10.3390/jmse9030323

Zuschin, M. and Stachowitsch, M. 2009. Epifauna-dominated benthic shelf assemblages: lessons from the modern Adriatic Sea. *PALAIOS*, **24**, 211–221, https://doi.org/10.2110/palo.2008.p08-062r